CELLULAR NEUROSCIENCE

The autism susceptibility kinase, TAOK2, phosphorylates eEF2 and modulates translation

Melad Henis[1,2]*, Tabitha Rücker[1], Robin Scharrenberg[1], Melanie Richter[1], Lucas Baltussen[3,4], Shuai Hong[1], Durga Praveen Meka[1], Birgit Schwanke[1], Nagammal Neelagandan[5,6], Danie Daaboul[3,4], Nadeem Murtaza[7,8], Christoph Krisp[9], Sönke Harder[9], Hartmut Schlüter[9], Matthias Kneussel[10], Irm Hermans-Borgmeyer[11], Joris de Wit[3,4], Karun K. Singh[7,12], Kent E. Duncan[5,13]*, Froylan Calderón de Anda[1]*

Genes implicated in translation control have been associated with autism spectrum disorders (ASDs). However, some important genetic causes of autism, including the *16p11.2* microdeletion, bear no obvious connection to translation. Here, we use proteomics, genetics, and translation assays in cultured cells and mouse brain to reveal altered translation mediated by loss of the kinase TAOK2 in *16p11.2* deletion models. We show that TAOK2 associates with the translational machinery and functions as a translational brake by phosphorylating eukaryotic elongation factor 2 (eEF2). Previously, all signal-mediated regulation of translation elongation via eEF2 phosphorylation was believed to be mediated by a single kinase, eEF2K. However, we show that TAOK2 can directly phosphorylate eEF2 on the same regulatory site, but functions independently of eEF2K signaling. Collectively, our results reveal an eEF2K-independent signaling pathway for control of translation elongation and suggest altered translation as a molecular component in the etiology of some forms of ASD.

INTRODUCTION

Translation of mRNA into protein is a tightly regulated step of gene expression that plays a key role in shaping the cellular proteome (*1*, *2*). Several well-described cellular signaling pathways mediated by protein kinases directly target the translational machinery via phosphorylation of translation initiation or elongation factors (*3*). Two of the best-characterized examples target translation initiation. Phosphorylation of eukaryotic initiation factor 4E–binding proteins (4EBPs) results in release of sequestered eIF4E, freeing it to associate with the mRNA cap structure to promote translation (*4*). Signaling via 4EBPs is mediated mainly by mammalian target of rapamycin complex 1 (mTORC1) in response to different cellular stimuli such as nutrient availability, cellular energy, stress, hormones, and growth factors (*5*). Conversely, phosphorylation of eukaryotic translation initiation factor 2α (eIF2α) on a single evolutionarily conserved serine leads to decreased availability of eIF2–guanosine triphosphate (GTP) for ternary complex formation (eIF2-GTP-tRNAiMet) required for start codon recognition and delivering the first methionine amino acid to the ribosome (*6*). eIF2α phosphorylation leads to general down-regulation of most translation, but paradoxically up-regulates proteins encoded by mRNAs with upstream open reading frames (*7*, *8*). In mammals, four kinases that can respond to different stress signals to phosphorylate eIF2α have been described (*9*). Elongation can also be targeted, with phosphorylation of eukaryotic elongation factor 2 (eEF2) on a conserved threonine (T56) reducing its binding to ribosomes and repressing translation elongation (*10*). In contrast to initiation factor regulation, to date, only a single kinase able to phosphorylate eEF2 has been described: eEF2K (*11*). Upstream inputs to eEF2K are well described and include calcium ions, calmodulin, and anabolic signaling pathways such as mTORC1, mitogen-activated protein kinases (MAPKs), and adenosine monophosphate–activated protein kinase (AMPK) that regulate eEF2K activity (*12*). Disturbances in the translational control machinery are implicated in several human diseases including cancers (*13*) and many neurological disorders, including neurodegeneration and autism spectrum disorders (ASDs) (*14*, *15*).

ASDs are a group of neurodevelopmental disorders with varying symptoms and severity, for which there is no single known cause. ASDs affect a high proportion of the human population, with an incidence of 1 in 54 children in the United States (*16*). Common symptoms in ASD individuals are impaired social interaction and cognition and repetitive behaviors (*17*). Several human disorders due to mutations in one single gene are often associated with cognitive abnormalities and are linked to autism. Moreover, the products encoded by the mutated gene in several monogenic disorders are associated with ASD symptoms and act as a repressor of protein synthesis (*18*). On the other hand, genetic studies have also shown an association between copy number variations (CNVs) and neurodevelopmental conditions, including ASDs (*19*). Such associations were frequently described for the human *16p11.2* locus, which contains

[1]Center for Molecular Neurobiology, University Medical Center Hamburg-Eppendorf, 20251 Hamburg, Germany. [2]Department of Anatomy and Embryology, Faculty of Veterinary Medicine, New Valley University, 72511 El-Kharga, Egypt. [3]VIB Center for Brain & Disease Research, Herestraat 49, 3000 Leuven, Belgium. [4]KU Leuven Department of Neurosciences, Leuven Brain Institute, Herestraat 49, 3000 Leuven, Belgium. [5]Neuronal Translational Control Group, Center for Molecular Neurobiology (ZMNH), University Medical Center Hamburg-Eppendorf (UKE), Falkenried 94, 20251 Hamburg, Germany. [6]Institute of Bioengineering (IBI), École Polytechnique Fédérale de Lausanne (EPFL), CH-1015 Lausanne, Switzerland. [7]Krembil Research Institute, Donald K. Johnson Eye Institute, University Health Network, 60 Leonard Ave, Toronto, Ontario M5T 0S8, Canada. [8]Department of Biochemistry and Biomedical Sciences, Faculty of Health Sciences, McMaster University, Hamilton, Ontario L8S 4A9, Canada. [9]Institute for Clinical Chemistry and Laboratory Medicine, Mass Spectrometric Proteomics Group, Campus Forschung, University Medical Center Hamburg-Eppendorf (UKE), 20246 Hamburg, Germany. [10]Institute of Neurogenetics, Center for Molecular Neurobiology, University Medical Center Hamburg-Eppendorf (UKE), 20251 Hamburg, Germany. [11]Transgenic Service Group, Center for Molecular Neurobiology (ZMNH), University Medical Center Hamburg-Eppendorf (UKE), Falkenried 94, 20251 Hamburg, Germany. [12]Faculty of Medicine, University of Toronto, Medical Sciences Building, 1 King's College Cir, Toronto, Ontario M5S 1 A8, Canada. [13]Evotec SE, Manfred Eigen Campus, Essener Bogen 7, 22419 Hamburg, Germany.
*Corresponding author. Email: melad.henis@gmail.com (M.H.); kent.duncan5@gmail.com (K.E.D.); fcaldero@gmail.com (F.C.d.A.)

31 genes (*20*). The *16p11.2* microdeletion is linked to ASDs and contributes to approximately 1% of all diagnosed cases of ASD (*21*). In contrast, reciprocal microduplications of *16p11.2* are associated with schizophrenia (*22*). However, it remains unclear which of the ~30 genes localized in the *16p11.2* region are causally linked to behavioral, functional, and anatomical changes observed in ASDs. Translation dysregulation has not been so far linked with this CNV, and none of the genes in the locus bear any obvious connection to translation.

The human *TAOK2* gene is localized in the *16p11.2* chromosomal region and has been implicated in neurodevelopmental disorders (*21*). TAOK2 is a serine/threonine kinase with two main spliced isoforms—the long TAOK2α isoform with 1235 amino acids and the shorter TAOK2β with 1049 amino acids. TAOK2α/TAOK2β isoforms share exons 1 to 16 (same residues 1 to 745) but differ at their C termini (*23*, *24*). Whole-genome and exome sequencing of ASD families identified de novo and inherited mutations in both TAOK2 isoforms (*25*). A Taok2-deficient mouse model has abnormalities in brain morphology and irregularities in synaptic and dendritic morphology (*25*). Moreover, these knockout mice showed abnormal postnatal hippocampal-prefrontal brain connectivity and impaired cognition and social behavior depending on *Taok2* dosage during adolescence (*25*).

Here, we show that TAOK2 interacts with the translational machinery and is present in polyribosome-mRNA translation complexes in cultured neurons and developing mouse brains. Moreover, we found that genetically altering TAOK2 levels affected translation, with protein synthesis increased in the absence of TAOK2 and reduced by TAOK2 overexpression, suggesting a previously undescribed function of TAOK2 as a translational repressor. This role requires the kinase activity of TAOK2, and we found that TAOK2 directly interacts with eEF2 to modulate its phosphorylation status on key regulatory sites. TAOK2 regulation is independent of the only known eEF2 kinase (eEF2K). Last, we found that cortices from the *16p11.2* deletion mouse model of ASD showed altered translation in vivo. Accordingly, cultured cortical neurons derived from those cortices presented exaggerated protein synthesis, which was rescued after reintroduction of TAOK2. Together, our results reveal an eEF2K-independent signaling pathway for control of translation elongation and suggest that translational control is associated with some forms of ASD (*18*, *26*).

RESULTS

Previously, we and others reported that, while TAOK2α is associated with microtubules (*23*, *27*), TAOK2β has a functional association with the actin cytoskeleton through binding to and affecting RhoA activity (*25*). However, the role of TAOK2 in neuronal differentiation is still not well understood. Here, we used a complementary combination of open-ended screening approaches to gain further insight into the functions of TAOK2 in the developing nervous system. First, we performed immunoprecipitation coupled with mass spectrometry (IP-MS) analysis using an anti-TAOK2β antibody in cytoplasmic lysates from either mouse cortices or N2a cells transfected with wild-type (WT) TAOK2β. In parallel, we used a neuronal proximity–based proteomic system to identify protein-protein interaction (PPI) networks associated with TAOK2β in mouse cortical neurons [18 days in vitro (DIV)] infected with lentiviral constructs, expressing a BioID2 fusion protein (pLV-hSyntGFP-P2A-TAOK2β-13xLinker-BioID2-3xFLAG) (*28*). Copurified proteins from the three biological samples were involved in chloride channel activity, synaptic structure constituents, and translational control based on gene ontology (GO) term analysis (Fig. 1 and table S1). Moreover, a detailed analysis of potential translational involvement of TAOK2β revealed connections to RNA processing, translation initiation, and translation elongation (fig. S1).

To investigate whether TAOK2β is associated with polyribosome translation complexes, we first performed polysome profiling from mouse cortices. Proteins were extracted from collected gradient fractions and used for immunoblotting analysis with antibodies against TAOK2β and control proteins. This showed the presence of TAOK2β in polysomes of WT mice and its absence in polysomes of *Taok2* knockout mice (Fig. 2A). The detected TAOK2β signal across the translationally active polysome-associated mRNAs (heavy polysomes) coincided with the distribution of the cytoplasmic poly(A)-binding protein 1 (PABP1) and large ribosomal subunit protein RPL7a, which served as positive controls. Moreover, we quantified the enrichment of TAOK2β in polysomes and found that TAOK2β is more enriched in fractions 1 to 8 than the other polysome fractions, a pattern observed with many translation factors (fig. S2, A and B, and table S7). To confirm the specific association of TAOK2β with polysomes, the cytoplasmic lysates from WT mouse cortices were treated with the Mg^{2+}-chelating agent EDTA to disrupt polysomes before loading on the sucrose gradient. The EDTA-treated profile showed the disappearance of polysomes due to the dissociation of ribosomes from the polyribosome complex following treatment. In contrast, the peaks of monosomes (the 80*S*) and ribosomal subunits 40*S* and 60*S* were increased (fig. S2C). Immunoblot analysis of the fractionated gradients from EDTA-treated profiles revealed a clear shift of TAOK2β signal from the heavier polysome fractions to the lighter fractions (unbound ribosomal subunits and monosomes). The shift of TAOK2β that coincided with that of PABP1 and RPL7a toward the lighter gradient fractions upon EDTA treatment suggests the presence of TAOK2β in polysomal fractions. EDTA sensitivity supports the idea that the TAOK2 signal in these fractions reflects polysome association, rather than spurious co-sedimentation with large, nonribosomal complexes (fig. S2, D and E). Together, these data demonstrate the specific association of TAOK2β with ribosome-mRNA translational complexes.

We next examined whether the presence of TAOK2 in polyribosome complexes might be isoform specific. Specifically, we transiently transfected N2a cells with plasmids expressing either Myc-tagged TAOK2α or TAOK2β isoform and tested for their presence in polysome fractions by immunoblotting. Immunoblot analysis revealed the presence of both α and β isoforms in the collected polysome fractions across the gradient (fig. S2, F and G). However, the Myc-tag signal of TAOK2α was less pronounced in heavy polysomes compared with the Myc-tag signal of TAOK2β that localized in both light and heavy polysomes. Moreover, we determined the amount of each Taok2 isoform in polysomes from mouse cortices. To this end, we performed liquid chromatography with mass spectrometry coupling (LC-MS/MS) analysis of the extracted proteins from polysomes. We found that TAOK2β was more abundant in polysomes (65.21%) than TAOK2α (34.79%) (fig. S2H and table S2), suggesting more enrichment of TAOK2β in polysomes than TAOK2α. Collectively, these data demonstrate that both isoforms associate with polysomal fractions, but the relative distribution across fractions might be different for the two isoforms.

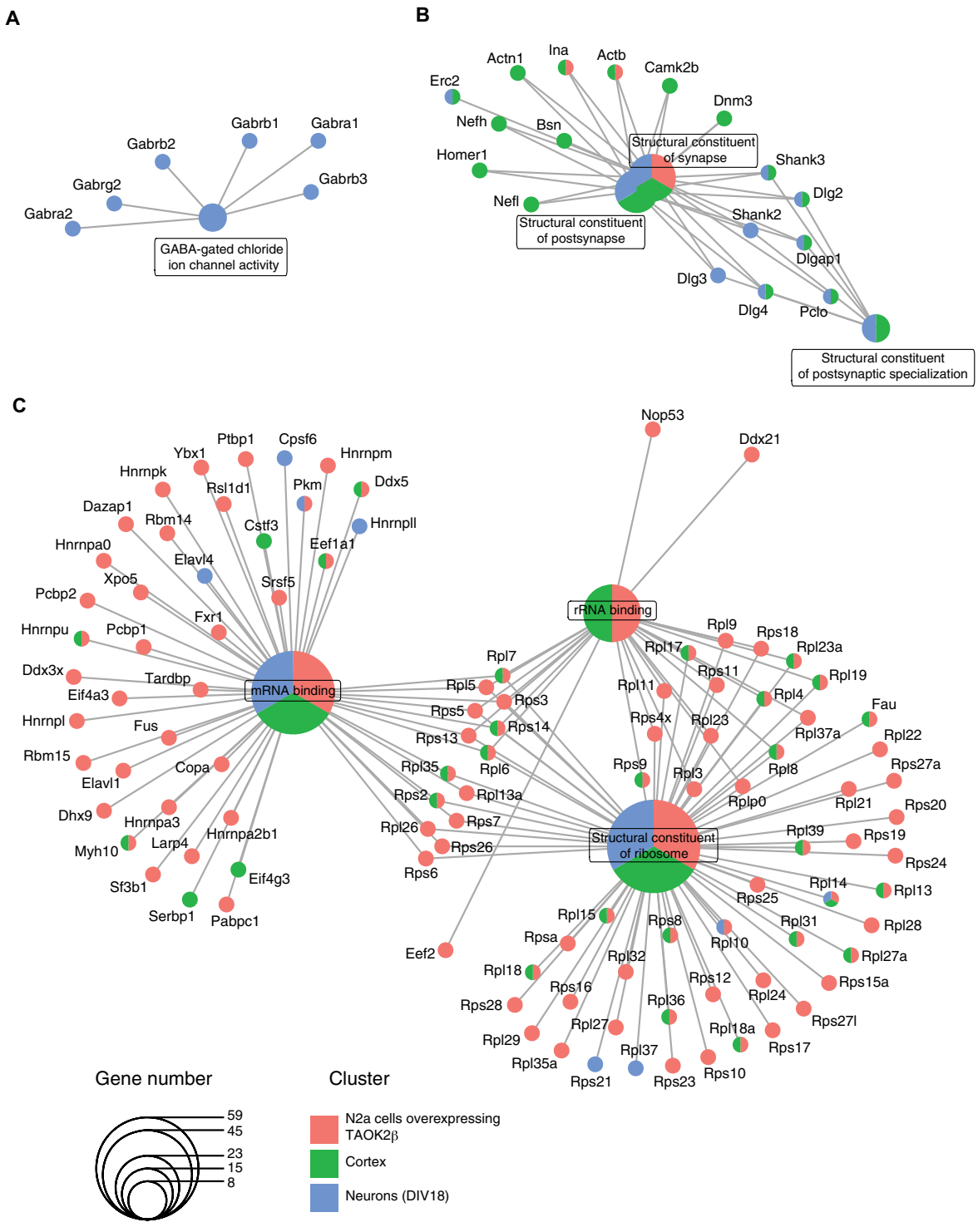

Fig. 1. TAOK2β associates with proteins involved in translational regulation, neuronal synaptic structure, and GABA-gated chloride ion channel activity. Over-representation analysis as cnetplot of the filtered MS-detected proteins that were copurified by an anti-TAOK2β antibody from lysates of N2a cells overexpressing TAOK2β (red), mouse cortex (green), and DIV18 cortical neurons (blue, neuronal proximity–based proteomic system) shows GO enrichments for GABA-gated chloride ion channel activity (**A**) and structural constituents of synapses (**B**). GO enrichment for mRNA binding, ribosomal RNA binding, and structural constituents of the ribosome (**C**) are all functionally related to translational regulation. Circle size indicates the number of genes associated with the respective GO enrichments (details in table S1), and color indicates the respective biological samples used for GO enrichments.

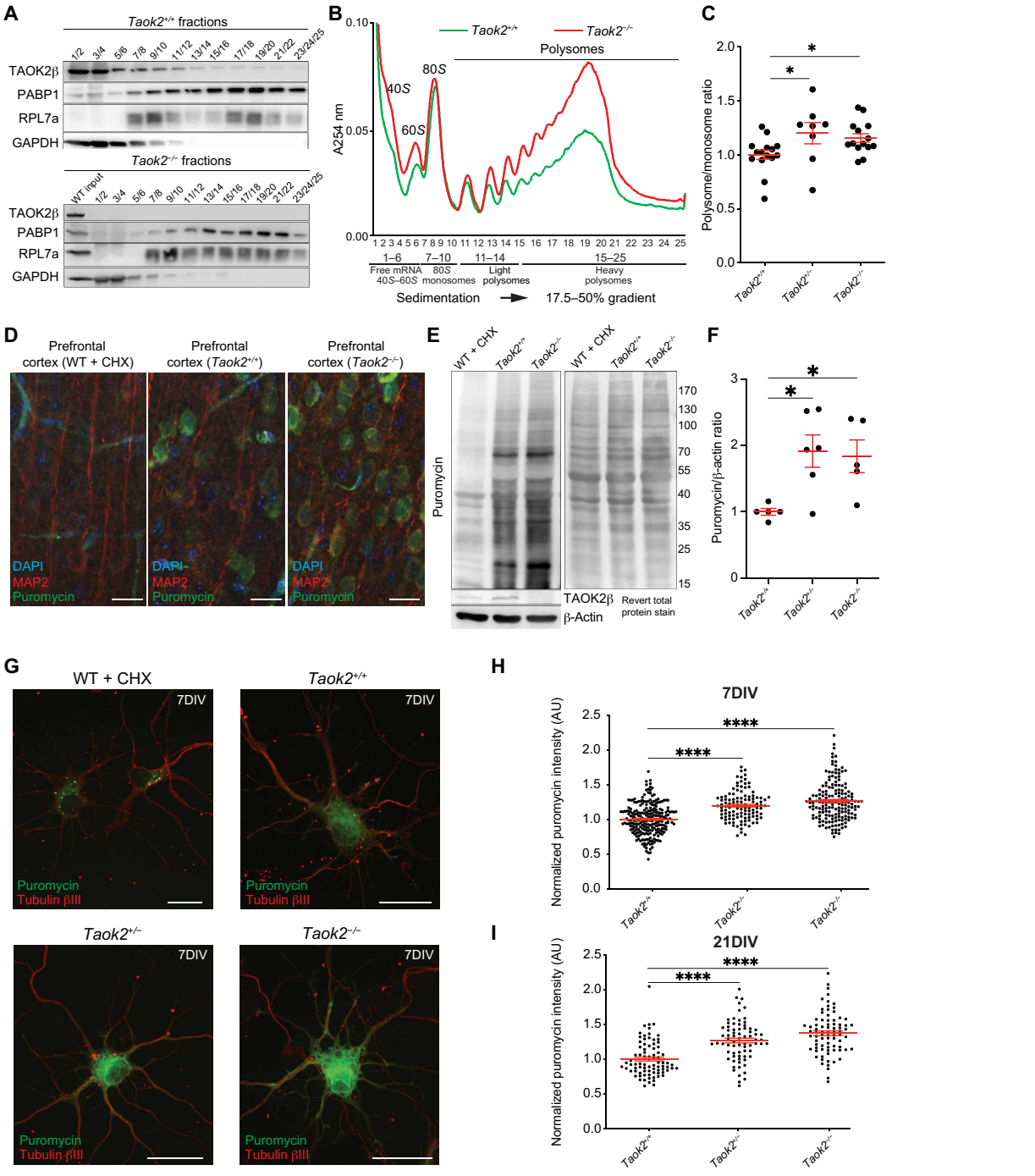

Fig. 2. TAOK2β associates with the polyribosome complex, and its deficiency enhances general translation and protein synthesis. (**A**) Immunoblots of polysome fractions showing the presence or absence of TAOK2β across all polysome fractions isolated from *Taok2*$^{+/+}$ (top) or *Taok2*$^{-/-}$ (bottom) mouse cortex. PABP1, RPL7a, and glyceraldehyde-3-phosphate dehydrogenase (GAPDH) were used as positive and negative controls, respectively, to prove polysome preparation efficiency. (**B**) Polysome profiles from *Taok2*$^{+/+}$ and *Taok2*$^{-/-}$ mouse cortices. (**C**) Quantification of polysome profiles in *Taok2*$^{-/-}$, *Taok2*$^{+/-}$, and *Taok2*$^{+/+}$ mice cortices. *Taok2*$^{+/+}$, $n = 13$; *Taok2*$^{+/-}$, $n = 8$; *Taok2*$^{-/-}$, $n = 12$; scanning electron microscopy (SEM) error bars, ordinary one-way analysis of variance (ANOVA) ($P = 0.0251$) followed by Dunnett's multiple comparisons test (*$P < 0.05$). (**D**) Immunostainings of acute cortical slices from the prefrontal cortex of *Taok2*$^{+/+}$ and *Taok2*$^{-/-}$ mice analyzed by SUnSET assay. WT slices pretreated with the translation inhibitor cycloheximide (WT + CHX) verifies the specificity of the puromycin antibody signal. (**E**) Immunoblot from acute cortical slices analyzed by SUnSET assay. (**F**) Quantification from (E). *Taok2*$^{+/+}$, $n = 5$; *Taok2*$^{+/-}$, $n = 6$; *Taok2*$^{-/-}$, $n = 5$; SEM error bars, ordinary one-way ANOVA ($P = 0.0167$) followed by Dunnett's multiple comparisons test (*$P < 0.05$). (**G**) Immunostainings of primary neurons (7DIV) analyzed by SUnSET assay. Cultured WT neurons were pretreated with CHX (WT + CHX). (**H** and **I**) Quantifications of immunofluorescent SUnSET assay of 7DIV neurons or 21DIV. 7DIV cells: *Taok2*$^{+/+}$, $n = 236$ (five embryos); *Taok2*$^{+/-}$, $n = 113$ (four embryos); *Taok2*$^{-/-}$, $n = 166$ (four embryos). 21DIV cells: *Taok2*$^{+/+}$ (three embryos), $n = 81$; *Taok2*$^{+/-}$, $n = 73$ (two embryos); *Taok2*$^{-/-}$, $n = 79$ (three embryos). SEM error bars, ordinary one-way ANOVA ($P < 0.0001$) followed by Dunnett's multiple comparisons test (****$P < 0.0001$). Scale bars, 10 μm [(D) and (G)].

Next, we aimed to assess the effect of *Taok2*-dependent regulation of translation in brain tissues. Therefore, we performed polysome profiling from cortices of *Taok2*-deficient mice (*Taok2*$^{-/-}$ and *Taok2*$^{+/-}$). Polysome/monosome (P/M) ratios, which indicate the cellular translational state, revealed that the absence of *Taok2* leads to significant changes in global translation. Cortices from *Taok2*-deficient mice exhibited increased P/M ratios, strongly suggesting enhanced translation in the *Taok2*-deficient mice (Fig. 2, B and C).

Changes in ribosome density in polysome assays imply effects on the translational machinery but do not necessarily reflect corresponding directional effects on protein synthesis. For example, increased ribosome density could be due to more ribosomes actively translating, enhanced ribosome stalling, or failure to clear defective ribosomes via quality control mechanisms (*1*, *29*). To distinguish between these scenarios and gain more insight into how TAOK2 affects protein synthesis, we used the surface sensing of translation "SUnSET" assay (*30*, *31*) to measure the global protein synthesis in acute brain slices from 4-week-old mice. Consistent with an increased P/M ratio from the polysome profiling, puromycin labeling of newly synthesized proteins was also increased in brain slices from *Taok2*$^{-/-}$ and *Taok2*$^{+/-}$ mice as compared to *Taok2*$^{+/+}$ mice (Fig. 2, D to F). To determine whether protein synthesis is enhanced in neurons, we cultured cortical neurons from *Taok2*$^{-/-}$, *Taok2*$^{+/-}$, and *Taok2*$^{+/+}$ mice. At DIV7 or DIV21, cultured neurons were treated with puromycin to label the newly synthesized proteins, and quantitative immunofluorescent SUnSET analysis was performed. Consistent with what we found in cortical slices, *Taok2*$^{-/-}$ and *Taok2*$^{+/-}$ neurons showed a significant increase in the incorporated puromycin signal at the soma compared to the control *Taok2*$^{+/+}$ neurons (Fig. 2, G to I), reflecting increased neuronal protein synthesis. Moreover, gene set enrichment analysis (GSEA) of the *Taok2*$^{-/-}$ total proteome in different brain regions confirmed our previous findings that translation is affected, with many ribosomal proteins being significantly up-regulated throughout the brain (fig. S7, B and C, and table S3). These data demonstrate that neurons lacking *Taok2* have increased protein synthesis.

We next asked whether the physical association of TAOK2 with mRNA-ribosome translation complexes reflects a functional role in regulating translation. To this end, we expressed mutated loss-of-function TAOK2β or TAOK2α [containing an A135P mutation, a human de novo missense mutation, which renders this protein into a kinase-dead form of TAOK2 (*25*)] in N2a cells and evaluated their polysome profiles. Quantification of polysome profiling assays revealed that the P/M ratios were significantly increased in cells expressing TAOK2β A135P relative to control cells but were not affected by TAOK2α A135P expression (fig. S3, A and F). This suggests that there are more ribosomes bound to cellular mRNAs after introducing the TAOK2β kinase-dead protein. Conversely, the P/M ratio was decreased after the introduction of WT TAOK2β or TAOK2α in N2a cells (fig. S3, G to I). These data point to a functional connection between TAOK2 kinase activity and translation regulation. Moreover, given that the A135P mutation leading to defective kinase activity was originally identified in a patient with ASD (*25*), it establishes a correlation between defective translation control and increased susceptibility to ASD.

Furthermore, SUnSET assay analysis (*31*) of N2a cells transfected either with WT isoforms (TAOK2β or TAOK2α) or with their respective kinase-dead constructs (TAOK2β A135P or TAOK2α A135P) showed decreased or increased levels of puromycin incorporation into newly synthesized proteins, respectively (fig. S4, A to F). Last, we used an ASD patient–derived lymphoblastoid cell line (LCL) expressing de novo mutations in TAOK2: TAOK2 A135P (present in both isoforms) and a C-terminal deletion (P1022*), present only in the TAOK2β isoform (*25*). Accordingly, polysome profiling and protein synthesis analysis from patient-derived LCLs with the A135P mutation revealed increased P/M ratios (fig. S5, A and B) together with increased levels of newly synthesized proteins, as determined by immunoblot of puromycin (fig. S5, C and D), compared to the cells derived from the nonaffected father. Similarly, the cells of the patient with the C-terminal P1022* deletion have both increased P/M ratios by polysome profiling analysis and increased global protein synthesis by SUnSET assay, as compared with the nonaffected father (fig. S5, E to H). Likewise, N2a cells expressing TAOK2β P1022* mutation showed increased P/M ratios by polysome profiling analysis (fig. S6, A to C). Together, these results demonstrate that TAOK2 regulates translation as a repressor of protein synthesis in N2a cells and ASD patient–derived LCL cells.

Global protein synthesis is regulated by many different processes but especially by phosphorylation of translation factors, ribosomal proteins, and other supporting proteins [e.g., RNA binding proteins (RBPs)] (*3*). Given that TAOK2 is a kinase and we found that its kinase activity was required for normal regulation of protein synthesis, we hypothesized that altered phosphorylation of specific translation machinery components or regulators would underlie the effects on translation. Thus, to understand how TAOK2 exerts its function as a repressor of translation, we used a labeled phosphoproteomics approach (fig. S7A) in multiple brain regions of *Taok2*$^{+/+}$, *Taok2*$^{+/-}$, and *Taok2*$^{-/-}$ mice to determine the potential phosphorylation targets of Taok2. Identified phosphorylation sites were filtered for the minimal kinase-recognition motif of TAOK2 pTXX[K/R/H] (*32*) to select for potential direct substrates of its kinase activity. High-confidence targets were expected to be significantly down-regulated in at least two *Taok2*$^{-/-}$ brain regions. Three phosphorylation sites met these requirements: LPPR3 Thr^{374}, CRMP1 Thr^{509}, and eEF2 Thr^{57} (Fig. 3A and table S4).

The phosphorylation status of elongation factor eEF2 is crucial in regulating translation at the elongation step, affecting ribosome translocation along the mRNA (*33*). Especially phosphorylation of residue Thr^{56} (corresponding to mouse Thr^{57}) is known to strongly inhibit eEF2 activity and thereby the rate of translation (*10*). Therefore, we validated the finding that eEF2 Thr^{57} phosphorylation is reduced in *Taok2*$^{-/-}$ mouse brains by using a well-established rabbit anti–phospho-eEF2 (Thr^{56}) antibody in mouse cortical lysates (Fig. 3, B and C). This phosphorylation is usually ascribed to eEF2K and has already been linked to fragile X syndrome (FXS) (*34*). Similarly, phosphorylation of eEF2 by TAOK2 could act as a potent elongation inhibitor in global protein synthesis.

According to our initial IP-MS approach, we also detected eEF2 in protein complexes immunoprecipitated with the TAOK2β antibody (Fig. 3D), confirming the result obtained after overexpression of TAOK2β in N2a cells (Fig. 1 and table S1). To determine whether TAOK2 can directly phosphorylate eEF2, we incubated bacterially purified His-tagged eEF2 protein with human purified glutathione *S*-transferase (GST)–tagged TAOK2 kinase domain (amino acids 1 to 314) in an in vitro kinase assay. We found that in the absence of other proteins, in particular eEF2K [as confirmed by LC/MS (table S5) and Coomassie staining and immunoblot (both in fig. S9)], small amounts of TAOK2 can already lead to phosphorylated eEF2

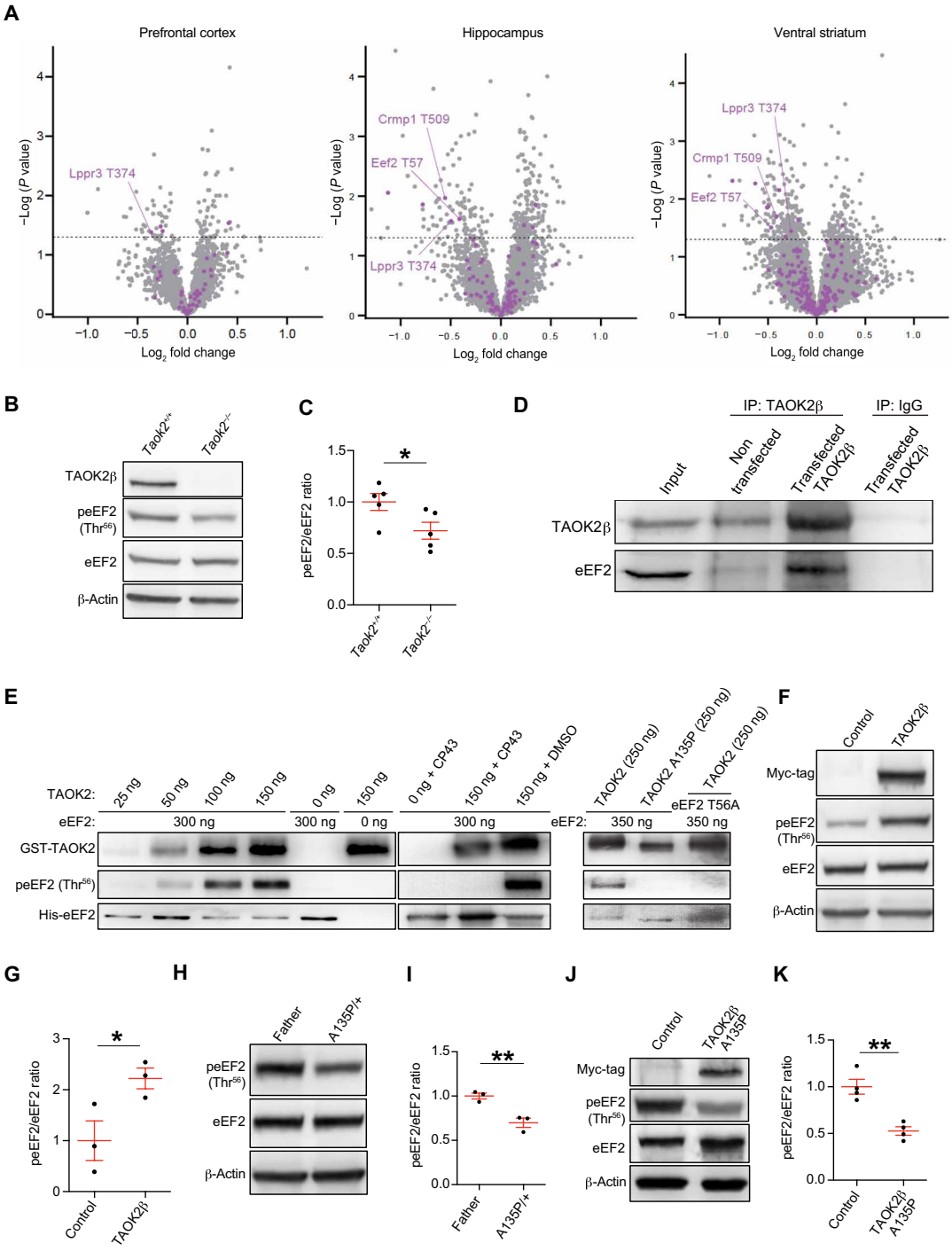

Fig. 3. TAOK2β binds eEF2 and represses translation through direct phosphorylation of its Thr^{56} residue. (**A**) Volcano plot of *Taok2* knockout/*Taok2* WT phosphoproteome (left, prefrontal cortex; middle, hippocampus; right, ventral striatum). Phosphopeptides containing the TAOK2 kinase-recognition motif pTXX[K/R/H] are in purple and highlight potential direct substrates of TAOK2. Two data points are outside of axis limits. (**B** and **C**) Immunoblot and quantifications of phosphorylated eEF2 (Thr^{56}) from cortical lysates from *Taok2*$^{+/+}$ and *Taok2*$^{-/-}$ mice ($n = 5$); *$P < 0.05$, SEM error bars, unpaired *t* test. β-Actin was used as a loading control. (**D**) Immunoblot of the TAOK2β IP from nontransfected N2a cells and N2a cells overexpressing WT TAOK2β shows the interaction of TAOK2β with eEF2. (**E**) Immunoblots of in vitro kinase assays using recombinant proteins as depicted in the figure show the direct phosphorylation of eEF2 (Thr^{56}) by TAOK2 kinase. (**F** and **G**) Immunoblot and quantifications of phospho-eEF2 from N2a cell lysates transfected with WT TAOK2β and its respective control (cells expressing pcDNA3.1-myc-tag). $n = 3$ per condition from different independent transfection experiments; *$P < 0.05$, SEM error bars, unpaired *t* test. (**H** and **I**) Immunoblot and quantifications of phospho-eEF2 from LCLs lysates with TAOK2 mutation A135P (patient) and the nonaffected father. $n = 3$ per condition; **$P < 0.05$; SEM error bars, unpaired *t* test. (**J** and **K**) Immunoblot and quantifications of phospho-eEF2 from N2a cell lysates transfected with TAOK2βA135P and its respective control (cells expressing pcDNA3.1-myc-tag). $n = 4$ per condition from different independent transfection experiments; SEM error bars, **$P < 0.01$ by unpaired *t* test. β-Actin was used as a loading control.

Thr^{56} in a dose-dependent manner. Two additional experiments support TAOK2 as the kinase mediating this effect. First, including CP43, a known inhibitor of TAOK2 kinase activity, eliminated phosphorylation of eEF2 (*35*). Second, a control kinase-dead TAOK2 protein containing the mutation A135P was expressed and purified in the same manner as WT active TAOK2 (fig. S9) but showed no eEF2 (Thr^{56}) phosphorylation (Fig. 3E). eEF2 (Thr^{56}) phosphorylation was not observed when the TAOK2 kinase domain was incubated with the mutated form of eEF2 (T56A) in the in vitro kinase assay (Fig. 3E). Collectively, these data demonstrate that phosphorylation of threonine-56 on eEF2 can be directly mediated by TAOK2. Consistent with these data, the overexpression of TAOK2β in N2a cells causes increased phosphorylation of eEF2 (Fig. 3, F and G) concomitant with decreased amounts of newly synthesized protein, assessed by puromycin labeling (fig. S4, B and D to F). On the contrary, we observed reduced phosphorylation of eEF2 (Thr^{56}) and increased levels of newly synthesized protein in ASD patient–derived LCLs containing the TAOK2 A135P mutation (Fig. 3, H and I, and fig. S5, C and D) and in N2a cells expressing TAOK2β A135P (Fig. 3, J and K, and fig. S4, C and D), thus suggesting a dominant negative effect of TAOK2 A135P. Moreover, we could not detect phosphorylation changes in the only known upstream kinase of eEF2, eEF2K (*10*) (table S4 and fig. S8), further suggesting that TAOK2 directly phosphorylates eEF2 rather than functioning upstream of eEF2K. Together, these results suggest that TAOK2 kinase activity inhibits eEF2 activity via phosphorylation of its Thr^{56} residue, leading to decreased protein synthesis. With the current data, we show that TAOK2 associates with polysomes and phosphorylates eEF2. However, we cannot say whether polysome association of TAOK2 is necessary for phosphorylation. Phosphorylation of eEF2 has been shown to affect its functional activity and reduce its binding affinity for ribosomes (*36*).

Since the human *TAOK2* gene is in the genomic ASD-associated *16p11.2* locus, we next asked whether the mouse model of the *16p11.2* deletion [B6;129S7- Del(7Slx1b-Sept1)4Aam/J$^{+/-}$, abbreviated as *16p11.2del*$^{+/-}$] would recapitulate our findings regarding dysregulated global translation. We analyzed the polysome profiles of cortices from a *16p11.2del*$^{+/-}$ mice (*37*) and found increased P/M ratios (Fig. 4, A and B), similar to our observations with cortices from *Taok2*$^{-/-}$ mice (Fig. 2, B and C), reflecting enhanced ribosome density on cellular mRNAs. Accordingly, cultured cortical neurons from the *16p11.2del*$^{+/-}$ mice treated with puromycin showed an elevated rate of puromycin labeling of the newly synthesized proteins compared to WT cells (Fig. 4, C to E). Our results provide clear evidence that TAOK2 is a translation repressor; therefore, we aimed to rescue the effect of enhanced translation in the*16p11.2del*$^{+/-}$ mouse model. We generated a transgenic mouse B6;129S7-*(Del(7Slx1bSept1) Tg(TaoK2Hhtg)*Cal (abbreviated as *delTgTaoK2*), where *Taok2* was reintroduced in the *16p11.2del*$^{+/-}$ mouse model and cortices were analyzed by polysome profiling assay. The increased P/M ratios from *16p11.2del*$^{+/-}$ mouse cortices were normalized to WT levels by reintroduction of *Taok2* on a transgene (Fig. 4, F to H), implying that *TAOK2* alone is likely to mediate the impact of *16p11.2* deletion on translation. Last, we tested whether the TAOK2β alone could rescue the exaggerated protein synthesis phenotype in *16p11.2del*$^{+/-}$ neurons. To this end, we used in utero electroporation (IUE) to transfect *16p11.2del*$^{+/-}$ cortices with TAOK2β and tDimer at embryonic days 14.5 to 15 (E14.5 to E15) and prepared primary cortical neuronal cultures 2 days later (E17). After 7DIV, cultured neurons were treated with puromycin to label the newly synthesized proteins and prepared for immunostaining using puromycin and TAOK2β antibodies. Notably, after the reintroduction of TAOK2β, the levels of newly synthesized proteins were reduced (Fig. 4, I and J), confirming the role of TAOK2β as a repressor of protein synthesis.

Together, our results demonstrate a previously unknown role for TAOK2 in translational control of protein synthesis via interaction with the translational machinery and phosphorylation of the elongation factor eEF2. Moreover, we observe the same translation phenotypes in a mouse model for ASD caused by the *16p11.2* microdeletion. TAOK2 appears to be the key mediator of these translation phenotypes, given that reintroducing *TAOK2* transgenically or TAOK2β alone in neurons is sufficient for rescue. Thus, our data support altered translation as a feature of the *16p11.2* microdeletion, raising the possibility that this could contribute causally to ASD in patients with this genomic variant.

DISCUSSION

The ASD-susceptibility gene *TAOK2* associates with the translation machinery and represses translation

Translational control is important for gene expression in response to different physiological and pathological conditions (*38*). Many ASD-associated genes encode proteins that are components of the translational machinery and regulatory proteins involved in different stages of translation (e.g., eIF4E, eIF3g, eEF1A2, RPL10, eIF-4EBP2, and UPF3B) (*39*). Moreover, many RBPs, which regulate mRNA translation, are known ASD risk genes as well. For example, *FMRP*, a well-known ASD-associated gene, is one of the best-characterized RBPs functioning as a translational repressor, and its deficiency underlies the pathogenesis of FXS (*40*).

The strong connections between dysregulated translation factors and ASD have led to the proposal over a decade ago that failure to properly tune the levels of neuronal protein synthesis might be a fundamental cause of ASD (*18*, *41*, *42*). This idea is supported by more recent work demonstrating a key role for translation initiation regulatory pathways in mediating pathobiology in ASD models, as well as the potential to correct these pathways for therapeutic benefit (*26*, *43*, *44*). However, it has remained unclear whether *16p11.2* CNV–mediated ASD connects to translation; no gene in the locus encodes a protein previously implicated in protein synthesis or its regulation. Here, we show that a gene located in the ASD-associated *16p11.2* locus is associated with translational control. Specifically, we reveal that TAOK2 can act as a repressor regulating protein synthesis at the elongation step. Previously, different proteins involved in translation were among numerous proteins identified as potentially enriched binding partners of Taok2 using a peptide pull-down method from neuronal lysate (*45*). Our protein screen and analysis of purified polyribosome complex proteins using Taok2-specific antibodies confirmed the presence of Taok2 protein in polyribosome translation complexes. How exactly TAOK2 is recruited to polysomes remains an open question. Previous work has shown that the TAOK family proteins contain a double-stranded RNA binding domain that can mediate interactions with viral RNA (*46*). However, Taok2 was not identified as a noncanonical mRNA binding protein in the global mRNA interactome capture experiments (*47*, *48*). Translation involves dynamic interactions between multiple-subunit initiation factors, RBPs, and large protein-RNA complexes (i.e., the ribosome). We capture most of these in our pull-downs, and in principle, any of

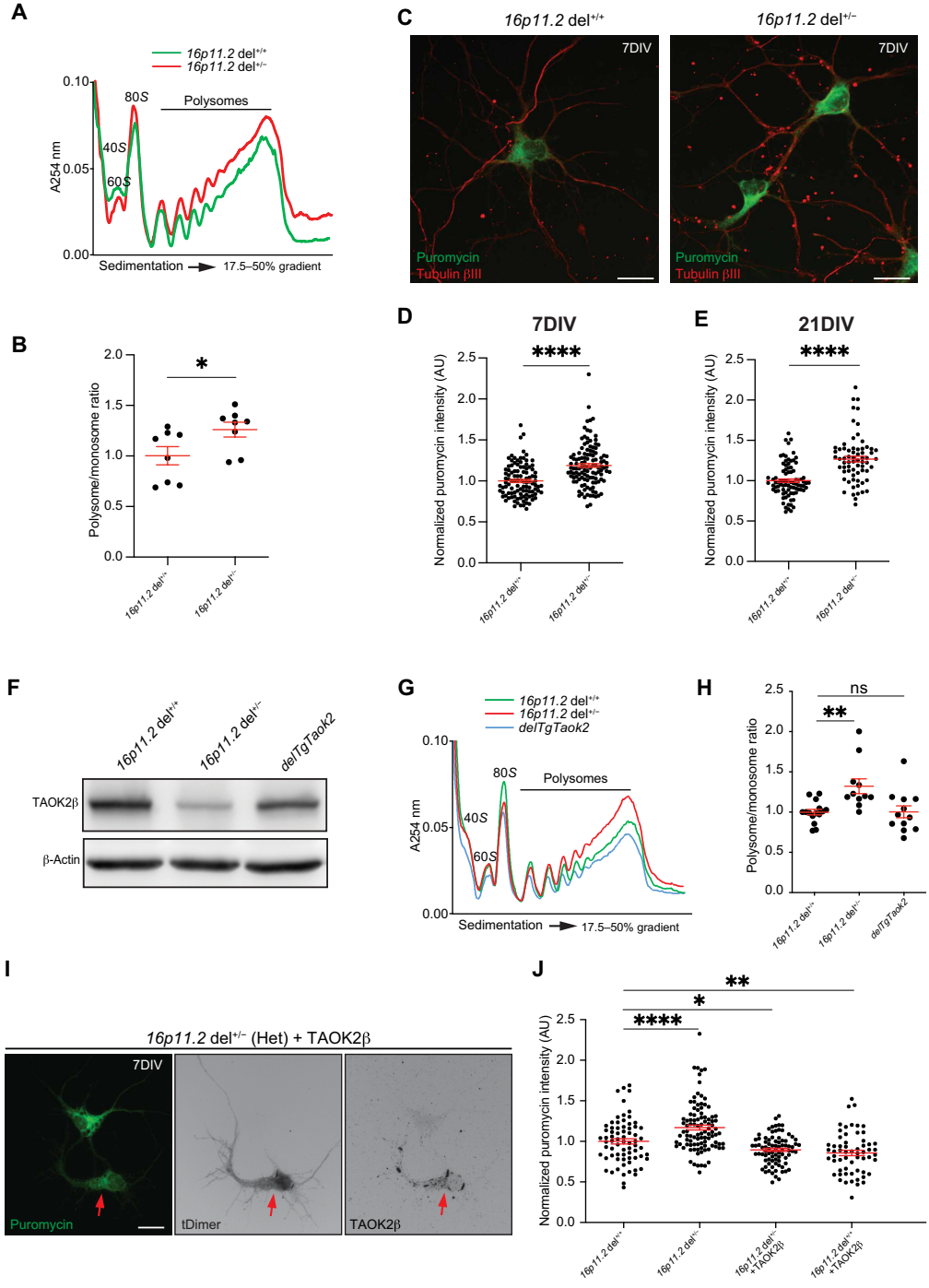

Fig. 4. *16p11.2* microdeletion displays dysregulated global translation that is rescued in the presence of TAOK2. (**A**) Polysome profiles from *16p11.2del*$^{+/+}$ and *16p11.2del*$^{+/-}$ mice cortices. (**B**) Quantification from (A). *16p11.2del*$^{+/+}$, $n = 8$ mice; *16p11.2del*$^{+/-}$, $n = 8$ mice; SEM error bars, $^{*}P < 0.05$ by unpaired *t* test. (**C**) Immunostainings of primary neurons 7DIV (*16p11.2del*$^{+/-}$) analyzed by SUnSET assay. (**D** and **E**) Quantifications of normalized puromycin labeling intensity of cultured neurons at 7DIV and 21DIV. 7DIV, *16p11.2del*$^{+/+}$: $n = 107$ (three embryos), *16p11.2del*$^{+/-}$: $n = 119$ (four embryos). 21DIV, *16p11.2del*$^{+/+}$: $n = 85$ (five embryos), *16p11.2del*$^{+/-}$: $n = 68$ (four embryos). SEM error bars, $^{****}P < 0.0001$ by unpaired *t* test. (**F**) Immunoblot shows the expression of TAOK2β in the cortices of *16p11.2del*$^{+/+}$, *16p11.2del*$^{+/-}$, and *delTgTaoK2* mice. (**G**) Polysome profiles from *16p11.2del*$^{+/+}$, *16p11.2del*$^{+/-}$, and *delTgTaoK2* mice cortices. (**H**) Quantifications of polysome profiles from (G). *16p11.2del*$^{+/+}$, $n = 15$ mice; *16p11.2del*$^{+/-}$, $n = 11$ mice; *delTgTaoK2*, $n = 13$ mice (one value was identified as an outlier). SEM error bars, ordinary one-way ANOVA ($P = 0.0021$) followed by Dunnett's multiple comparisons test ($^{**}P < 0.01$). (**I**) Immunostaining of *16p11.2del*$^{+/-}$ cortical neurons after IUE at E14.5 to E15 with TAOK2β and t-Dimer2 plasmids and treated at 7DIV with puromycin. (**J**) Quantifications from (I). Nontransfected *16p11.2del*$^{+/+}$, $n = 71$; *16p11.2del*$^{+/+}$ plus TAOK2β, $n = 60$ (four embryos); nontransfected *16p11.2del*$^{+/-}$, $n = 99$; *16p11.2del*$^{+/-}$ plus TAOK2β, $n = 84$ (four embryos). SEM error bars, ordinary one-way ANOVA ($P < 0.0001$) followed by Dunnett's multiple comparisons test ($^{*}P = 0.0329$, $^{**}P = 0.0051$, $^{****}P < 0.0001$). Scale bars, 10 μm [(C) and (I)].

them might recruit TAOK2. Regardless of how TAOK2 is recruited to the translational machinery, these data suggested a functional role for TAOK2 in regulation of translation, which we could substantiate via multiple lines of evidence.

A role for any *16p11.2* encoded gene in translation is particularly interesting, since several studies suggest that disturbances in the translational control machinery and the subsequent dysregulation of synaptic proteins are one of the molecular mechanisms underlying the etiology for synaptopathies in ASD (*18*, *26*). Therefore, dysregulated protein synthesis is considered a feature in some autistic phenotypes, and excessive neuronal protein synthesis is observed in FXS pathogenesis (*49*) and in other forms of autism (*26*, *43*). In this regard, measurement of the amount of newly synthesized protein by the SUnSET assay showed enhanced protein synthesis in cortex and neurons from *Taok2*-deficient mice compared to the WT controls. These data suggest that Taok2 is a repressor of neuronal translation, like many other known autism-linked genes, such as *FMRP*, *PTEN*, and *TSC1/2*. Mutations in these genes disturb translation repression, cause aberrant protein synthesis, and lead to autistic phenotypes (*50*–*52*). Consistently, analysis of de novo global protein synthesis in animal models of FXS and in different cell types derived from patients with FXS, such as lymphoblastoid cells, fibroblasts, and induced pluripotent stem cell (iPSC)–derived neural progenitors, revealed increased global protein synthesis due to the absence of translation repression by *FMRP* (*53*–*55*).

Similarly, we found that lymphoblastoid cells from an autistic patient with TAOK2 mutated at the residue A135P in the kinase domain, which leads to loss of TAOK2 kinase function, showed enhanced ribosome density on mRNAs by polysome profiling analysis and a corresponding increased amount of newly synthesized proteins compared to cells derived from the nonaffected father. These data indicate that the role of TAOK2 in translational repression is mainly achieved through its kinase function. Furthermore, N2a cells, a neural crest–derived cell line, transfected with WT TAOK2β or WT TAOK2α revealed reduced translation in polysome profiling and protein synthesis assays compared to the control. However, when these cells were transfected with the kinase-dead TAOK2β A135P mutation, global translation analyzed by polysome profiling and the amount of protein synthesis measured by puromycin incorporation were elevated in comparison with control cells, suggesting a dominant negative phenotype in the absence of kinase activity. Such a phenotype was also observed upon transfection of the TAOK2α A135P, which also showed increased protein synthesis compared to the control cells when analyzed by SUnSET immunofluorescence assay (fig. S4D). The lack of significant effect in polysome profiling with this isoform probably reflects lower overall sensitivity of the polysome assay, which analyzes the bulk population including both transfected and untransfected cells. Overall, our data suggest that the defects in translational control and global protein synthesis directly result from the loss of TAOK2 kinase function, irrespective of isoform. On the other hand, we did observe quantitative differences in relative abundance in polyribosome fractions for the two isoforms, with a greater proportion of TAOK2β than TAOK2α appearing to be stably associated with polyribosome fractions according to LC-MS/MS analysis of extracted proteins from polysomes of WT mouse cortices and by immunoblot analysis of polysomes from N2a cells transfected with WT TAOK2β or WT TAOK2α. Whether this has any functional significance remains to be determined. The difference in the C termini of both isoforms (*24*, *25*) might affect their association with polyribosomes differentially. More generally, the mechanism of recruitment of TAOK2 to polysomes and whether it needs to be polysome associated to regulate translation will require further investigation. In addition, the autoregulatory function of the C terminus (*56*, *57*) can affect translational regulation as observed for the P1002* mutation at the C terminus (specific for the TAOK2β isoform) in patient-derived LCLs with P1002* mutation and N2a cells expressing TAOK2βP1002* (figs. S5, E to H, and S6). Previously, we showed that the protein levels of both A135P and P1022* mutants are reduced (*25*), suggesting protein instability. However, the phosphorylated levels of the TAOK2P1022* mutant are not changed compared with the WT kinase when comparing the pTAOK2/TAOK2 ratios (*25*). Thus, overall, there is less TAOK2P1022* phosphorylated. Given that we do not know how the active form or phosphorylated TAOK2P1022* is compartmentalized, it could be that in our polysome fraction, P1022* is less phosphorylated producing a dominant negative effect. Together, our data demonstrate that TAOK2 physically associates with the translational machinery to modulate translation as a repressor. Our data further highlight the kinase activity as crucial for TAOK2 function in translational control.

Taok2 represses translation elongation via direct phosphorylation of eEF2

Protein kinases other than TAOK2 have long been known to phosphorylate different components of the translational machinery, especially the initiation and elongation factors (*3*). These phosphorylation events regulate the activity and interactions of these factors with other translational machinery components to thereby regulate translation (*3*). Previous work has implicated known phosphoregulatory pathways that modulate activity of translation initiation factors in in different neuropsychiatric disorders (*43*, *58*). Our work suggests that elongation can also be targeted and identifies TAOK2 as a direct regulator of eEF2. Previous work identified a single eEF2K that can phosphorylate eEF2 on its Thr^{56} residue to inhibit its role in ribosome translocation during translation elongation (*10*, *59*, *60*). eEF2K is a Ca^{2+}/CaM-dependent kinase with multiple regulatory phosphorylation sites that affect its activity in response to different signaling pathways (*12*). eEF2K activity is inhibited because of phosphorylation of the inhibitory sites: Ser^{78}, Ser^{366} (*61*), and Ser^{359} (*62*) mediated via mTORC1 signaling, and Ser^{359} and Ser^{366} mediated via the MAPK pathway (*61*, *63*). Conversely, phosphorylation of Ser^{500} by cyclic AMP (*64*) and Ser^{398} by AMPK (*65*) stimulates eEF2K activity. TAOK2 is a serine/threonine kinase, and we did not detect any phosphorylation changes in eEF2K regulatory sites by phosphoproteomics (table S4) or Western blot (WB) using a phospho-Ser^{366}–specific antibody (fig. S8) in our search for TAOK2 targets. This suggests that Taok2 does not directly or indirectly affect eEF2K activity. Furthermore, we showed that the Thr^{56} residue of eEF2 is a phospho-site modulated by Taok2 and confirmed direct phosphorylation at this site by TAOK2 kinase using an in vitro kinase assay. Thus, our study identifies TAOK2 as a kinase other than eEF2K that can directly modulate phosphorylation of Thr^{56} of eEF2. We thereby suggest a mechanism for regulation of translation elongation and tuning of neuronal protein synthesis via the activity of TAOK2.

Our data suggest that TAOK2 controls translation via the elongation factor eEF2; however, we acknowledge that other mechanisms might also contribute. For example, differential expression protein analysis for different brain regions from *Taok2* knockout

mice showed many significantly up-regulated proteins that are translational machinery components, especially ribosomal proteins (fig. S7C and table S3). Up-regulation of translation factors, including ribosomal proteins, has been reported in ASD patient–derived neuronal precursor cells and postmortem cortical tissues and iPSC-derived neural progenitor cells, as well as in nonneuronal cell types such as lymphocytes from patients with ASD (*66*–*68*). Thus, up-regulation of ribosomal proteins is a feature of ASD and might also contribute in some way to the translation phenotypes that we observe. Although we did not find evidence for altered phosphorylation of known regulators of initiation (4EBPs or eIF2α) in our phosphoproteomics studies, an additional effect of TAOK2 on translation initiation is nevertheless possible in principle. However, since we find effects on eEF2 phosphorylation at specific sites previously determined to affect translation elongation, the simplest interpretation of our data is that this mechanism contributes significantly to the translation phenotypes that we observe in the absence of TAOK2 and its kinase activity.

TAOK2 is a key mediator of protein homeostasis in *16p11.2* microdeletion ASD models

TAOK2 is one of ~30 genes located in the *16p11.2* chromosomal region and has been implicated in the etiology of ASD (*21*). Specifically, the *Taok2*-deficient mouse model has similar anatomical and behavioral abnormalities to those identified in *16p11.2* microdeletion mouse models and patients (*25*, *69*, *70*). In our study, we observed enhanced translation and protein synthesis in the *16p11.2* microdeletion, phenocopying what we observed in a *Taok2* knockout mouse model. We were able to normalize the translation phenotypes by the reintroduction of *Taok2* in the *16p11.2* microdeletion mouse model itself or by direct delivery of TAOK2β to primary neurons derived from that model. Together, our data suggest that *TAOK2* is a potential key mediator of protein synthesis abnormalities in carriers of the *16p11.2* CNV. Furthermore, our results highlight previously unappreciated exaggerated protein synthesis due to a lack of TAOK2-mediated translational control in this important genetic model of ASD. Thus, altered translation emerges as an aspect of ASD, even for genetic variants where the genes themselves do not obviously connect to classical translational control pathways. This suggests that modulation of translation via TAOK2 or other routes might potentially have therapeutic benefit in *16p11.2*-caused ASD. Our results also motivate examining whether TAOK2 kinase activity and its impact on eEF2 phosphorylation may be more generally involved in effects on translation in patients with ASD outside of the *16p11.2* variant population. TAOK2 mRNA is a target, and its regulation is under control of fragile X mental retardation protein (FMRP), making it a high-risk gene associated with CNVs (*71*). Furthermore, FMRP represses translation at the initiation step, where it binds with CYFIP1 and inhibits cap-dependent translation initiation by blocking the eIF4E-eIF4G interaction (*72*), as well as at the elongation step by stalling ribosomes on its target mRNAs (*71*). Thus, it will be particularly interesting in the future to investigate whether there are connections between elongation regulation by TAOK2 and FMRP, as well as potential interplay with effects on translation initiation. One could envisage altered translation caused via multiple unlinked routes involving effects on initiation, RBPs, or elongation. However, it seems equally likely that homeostatic mechanisms will involve cross-talk between these different translational regulatory pathways. It will be important to explore these possibilities in future work aimed at understanding the contribution of altered translation to ASD pathobiology and the therapeutic potential for targeting translation to help patients with ASD.

MATERIALS AND METHODS

Animals and animal welfare and approvals

Taok2$^{-/-}$ mice (B6, *TaoK2*^{tm1Heb}/Cal) (*25*) and *16p11.2del*$^{+/-}$ mice [B6;129S7-*(Del(7Slx1b-Sept1)4*^{AaM}/Cal, Jax, no. 013128] (*37*) were bred as previously described. All animals were raised, genotyped, and housed in compliance with standard regulations at the Central Animal Facility at University Medical Center Hamburg-Eppendorf, Hamburg (UKE). All mice experiments were performed according to the German and European Animal Welfare Act. The used experimental procedures have the approval of the Animal Research Ethics Board (AREB), the local authorities of the State of Hamburg (TVA, N007/2018), and the animal care committee of UKE.

Generation of the B6;129S7-(DelSlx1bSept1)4Aam*Tg*TaoK2Hhtg/Cal mouse line

To introduce the mouse *Taok2* gene in the *16p11.2del* background, heterozygote zygote donor mice were obtained by breeding B6;129S7-(DelSlx1bSept1)4Aam (Jax, no. 013128) +/− to WT littermates. Superovulation and pronuclear injection were performed as described before (*73*).

The donor plasmid RP23-321H3_bb_Taok2 PB3′Amp_PB5′Kan was generated by Gene Bridges (now Gen-H, Heidelberg, Germany) (fig. S10) to allow target integration by PiggyBac transposase. PiggyBac integration sites flank 21.2-kb murine genomic DNA (chromosome 7: 126,464,301-126,485,468 of GRCm39 reference genome from ENSEMBL) covering the murine *Taok2* gene. For further use for a knock-in approach, flanking regions of the mouse locus on chromosome 7 corresponding to the human *16p11.2* locus were recombined at the 5′ and 3′ of the inverted terminal repeat (ITR) sites. The *Super PiggyBac Transposase* plasmid (System Biosciences; catalog no. PB210PA-1) was obtained from BioCat, Heidelberg. Integration of the insert by recombination was confirmed by polymerase chain reaction (PCR) using 5′-ITR–specific primer PB5-F (GTGCTTGTCAATGCGGTAAGTGTCACTG) with insert-specific primer *Taok*-rev (GGCATACATTCTTGGAGTCAACTTTACATTGC) and with 3′-ITR–specific primer PB3-rev (GCATGTGTTTTATCGGTCTGTATATCGAGG) with insert-specific primer *Taok*-F (CACTTTTTGTAATAGGTCTTCTAAACTCAGAAGTG).

To establish the B6;129S7-(DelSlx1bSept1)4Aam*Tg*TaoK2Hhtg/Cal mouse line, founder #31 was crossed to B6;129S7$^{+/+}$ obtained from matings of *16p11.2del*$^{+/-}$ to WT littermates and offspring was analyzed as described above. Animals carrying the TaoK2 insertion on the *16p11.2del*$^{+/-}$ background were crossed to *16p11.2del*$^{+/-}$ to obtain mice positive for the transgene on *16p11.2del*$^{-/-}$ background.

To confirm the *Taok2* insertion on the *16p11.2del*$^{+/-}$ background animals, genotypes were determined by PCR from mouse-tail DNA using standard protocols. First, the *16p11.2del* genotype was determined using the following primers: forward primer (CCTGAGCCTCTTGAGTGTCC) and reverse primer (GTCGGTTCAGGTGGTAGACG) for the WT allele, and forward primer (ACCTGGTATTGAATGCTTGC) and reverse primer (TGGTATCTCCATAAGACAGAATGC) for the mutant allele. Second, the *delTgTaoK2* genotype was determined with the following

primers: for the 5′ end, forward primer #956 PBTP5-FL (GTCCTTGTCAATGCGGTAAGTGTCACTG) and reverse primer #957 TAOK-5′-PBTP-rev (GGCATACATTCTTGGAGTCAACTTTACATTGC); for the 3′ end, forward primer #1090 TaoK-3-F2 (CACTTTTTGTAATAGGTCTTCTAAACT) and reverse primer #958 PBTP3-revL (GCATGTGTTTTATCGGTCTGTATATCGAGG).

Plasmids

WT TAOK2α and TAOK2β isoforms and their site-directed mutagenesis plasmids that have been described before (*25*) were used for N2a cell transfection in addition to pCDNA3.1-myc (as empty vector control plasmid) and pEGFP-F [plasmid encoding the enhanced green fluorescent protein (GFP) sequence with a farnesylated signal]. pAAV-CAG huTAOK2β WT (plasmid encodes humanTAOK2-short variant) and pAAV-CAG-tDimer2 [plasmid encodes the A tandem dimer mutant of DsRed tagged to the red fluorescent protein (RFP)] were used for IUE of cortical neurons. pLV-hSyn-tGFP-P2A-POI-13xLinker-BioID2-3xFLAG construct expressing BioID2 fusion proteins and Luciferase-P2A-BioID2-3xFLAG construct as a negative control were used in neuron viral infection (*74*).

Antibodies

The following antibodies were used in these studies for immunocytochemical or WB analysis: rabbit anti-Taok2β (Synaptic Systems, 395003; WB, 1:1000; Immunocytochemistry (ICC), 1:250; IP, 1:100); mouse anti-puromycin, clone 12D10 [Millipore, MABE343; WB, 1:10,000; immunohistochemistry (IHC); ICC, 1:5000]; chicken anti-MAP2 (Synaptic Systems, 188006; IHC, 1:500); guinea pig anti–β3-tubulin (Tuj1) (Synaptic Systems, 302304; ICC, 1:500); mouse anti–β-actin (Sigma-Aldrich, A5316; WB, 1:2000); rabbit anti–β-actin (13E5) (Cell Signaling Technology, 4970; WB, 1:5000); rabbit anti–Myc-tag (71D10) (Cell Signaling Technology, 2278; WB, 1:1000; ICC, 1:300); rabbit anti–immunoglobulin G (IgG) (Millipore, 03-241; IP, 1:200); rabbit anti–phospho-eEF2 (Thr^{56}) (Cell Signaling Technology, 2331; WB, 1:1000); rabbit anti–GST-tag (Cell Signaling Technology, 2625; WB, 1:1000); mouse anti–His-tag (27E8) (Cell Signaling Technology, 2366; WB, 1:1000); rabbit anti–His-tag (Cell Signaling Technology, 2365; WB, 1:1000); mouse anti-eEF2, clone 4B3-G7-H5 (Abcam, ab131202; WB, 1:2000); rabbit anti–phospho-eEF2K (Ser^{366}) (Cell Signaling Technology, 3691; WB, 1:1000); rabbit anti-RPL7a (E109) (Cell Signaling Technology, 2415; WB, 1:1000); rabbit anti-PABP1 (Cell Signaling Technology, 4992; WB, 1:1,000); and mouse anti-eEF2K antibody (C-12) (sc-390710; WB, 1:200). Horseradish peroxidase (HRP) (Dianova; WB 1:2000 to 5000) and Alexa Fluor 488–or 647–or 568–conjugated secondary antibodies (Invitrogen; ICC, 1:500; IHC 1:300) were also used. Nuclei were visualized with Hoechst (4′,6-diamidino-2-phenylindole) (DAPI) (Invitrogen; 3258, ICC/IHC, 1:5000).

In utero electroporation

Lateral ventricles of each embryo (E14.5 to E15) of pregnant *16p11.2del*$^{+/-}$ mice were microinjected with a combination of TAOK2β (2.5 μg/μl) and tDimer2 plasmids (0.3 μg/μl) as previously described (*25*). After surgery, the animals received meloxicam orally (10 to 20 mg/kg body weight, twice daily) in soft food to relieve postoperative pain until they were euthanized for embryo collection.

Cell lines

N2a cells were grown in Dulbecco's modified Eagle's high-glucose GlutaMAX culture medium (Invitrogen), supplemented with 10% fetal bovine serum (FBS; Gibco), 1% penicillin-streptomycin antibiotics (Invitrogen), and 2 mM L-glutamine (Invitrogen). N2a cells were transiently transfected with jetOPTIMUS DNA Transfection Reagent (Polyplus, catalog no. 117-15) according to the manufacturer's guidelines. The total amount of plasmid DNA used for transfection of a 10-cm plate was 9 to 10 μg [7 to 8 μg from different TAOK2 variants or empty vector control (pcDNA 3.1) + 2 μg of pEGFP-F plasmid]. Following 4 hours of transfection, the medium containing the transfection complex was replaced by a prewarmed fresh medium. Two hours later, the cells were passaged one time into 10-cm dishes or Poly-L-lysine (PLL) precoated glass coverslips, depending on the experimental conditions. The transfection efficiency was determined directly before harvesting by taking images for GFP-expressed signal in control and transfected cells or by IHC staining using antibodies against the Myc-tag protein or TAOK2β. Only cells with 70 to 80% transfection efficiency were harvested after 40 to 48 hours after transfection and used for experiments.

LCLs were generated from peripheral blood, mainly mononuclear cells confined from the blood of probands and their families, which were immortalized using the Epstein-Barr virus (*75*). LCLs were grown in a standard suspension condition in RPMI 1640 medium (PAN Biotech) supplemented with 15% FBS. Cells (200,000/ml) were used for starting a culture in 5 ml, and every 2 to 3 days, the medium was increased to 20 ml, and the cells were split to avoid overconfluency as they are growing in clumps. During the experiments, the cells were sedimented by centrifugation at 1000 rpm for 5 min at room temperature (RT).

Primary cortical neuron culture

Primary cortical neuron cultures from embryos of pregnant *Taok2*$^{+/-}$ or *16p11.2del*$^{+/-}$ mice were prepared as described previously (*25*). The cells were kept in culture for 7DIV or 21DIV at 37°C with 5% CO_2 before treatment with puromycin to measure protein synthesis by SUnSET assay. Cytosine β-D-arabinofuranoside (0.5 μM) was added to the cultured cells on 7DIV to the cells maintained up to 21DIV to inhibit the growth of the glia cells. Cortices of *16p11.2del*$^{+/+}$ and *16p11.2del*$^{+/-}$ embryos transfected with a combination of TAOK2β and tDimer2 plasmids via IUE at E14.5 to E15 were isolated 2 days later. The transfected cortical regions were identified by the red fluorescent signal and dissected on a cold surface under a stereomicroscope (Olympus SZX16) connected to an ultraviolet light source. Afterward, the cells were prepared and cultured for 7DIV.

Polysome profiling

Frozen dissected cortices (prefrontal and somatosensory) from both genders of 4-week-old *Taok2*$^{+/+}$, *Taok2*$^{+/-}$, and *Taok2*$^{-/-}$ mice or *16p11.2del*$^{+/+}$, *16p11.2del*$^{+/-}$, and *delTgTaoK2* mice were used for profiling. Polysome profiling was conducted as previously described (*76*), and 10 mM $MgCl_2$ was used in preparation of the sucrose gradients. To confirm the association of TAOK2β with polysomes, we followed the standard procedures used for polysome profiling of the cortex, and EDTA was added directly to the precleared cytoplasmic lysates (final concentration, 30 mM), which were maintained on ice

for 10 min before loading into the sucrose gradient before centrifugation.

Forty-eight hours, posttransfected and control N2a cells with 70 to 80% confluency at the harvesting time were treated with cycloheximide (CHX;100 μg/ml) at 37°C for 3 min before lysis. Cells were washed twice with ice-cold 1× phosphate-buffered saline (PBS) containing CHX (100 μg/ml). The cells were gently scraped from the plate in the residual PBS/CHX with a cell scraper. The cells from two 10-cm plates for each gradient were pooled together and spun down at 1000*g* for 5 min at 4°C. A cold lysis buffer containing 20 mM tris-HCl (pH 7.4), 100 mM KCl, 5 mM $MgCl_2$, 0.5 mM dithiothreitol (DTT), CHX (100 μg/ml), RNAsin (40 U/ml), Superasin (20 U/ml), Turbo deoxyribonuclease I (25 U/ml; Invitrogen), 1% NP-40, 1% Triton-X 100, 1× cOmplete protease inhibitor cocktail (Roche), and phosSTOP (Roche) was added to the pelleted cells and incubated on ice for 10 min. Afterward, the cells were triturated 10 times using a 27-gauge syringe, and the lysates were cleared by centrifugation at 2000*g* for 3 min followed by 16,900*g* for 7 min. The cleared cytoplasmic supernatants were transferred into an ice-cold microcentrifuges tube, the optical density at 260 nm (OD_{260}) of each lysate was measured, and equal OD unit volumes were loaded into 17.5 to 50% sucrose gradients prepared in a buffer containing 20 mM tris-HCl (pH 7.4), 100 mM NaCl, 5 mM $MgCl_2$, 1 mM DTT, and CHX (100 μg/ml). Sucrose gradient preparation, sample ultracentrifugation, gradient profiling, and collections of the fractions were done as previously described (*76*).

LCLs (1.5×10^9 to 2.0×10^9 per gradient) were spun down by centrifugation at 1000 rpm at RT and then treated with a prewarmed medium supplemented with CHX (100 μg/ml) at 37°C for 5 min. After CHX treatment, the cells were pelleted by centrifugation at RT and washed two times with ice-cold 1× PBS supplemented with CHX (100 μg/ml). The pelleted cells were lysed in the same polysome lysis buffer used for lysis N2a cells containing 10 mM $MgCl_2$ and profiled under similar conditions. P/M ratio was calculated as described previously (*76*). The P/M ratios generated from profiles of a certain experiment were normalized to the mean P/M ratio of the control profiles within the same experiment followed by statistical analysis for all pooled replicates.

Measurement of protein synthesis by SUnSET assay

Puromycin treatment

To measure the protein synthesis in the acute brain slices, we followed a previously described protocol (*30*, *31*). Briefly, 400-μm coronal brain slices were prepared from 4-week-old *Taok2*$^{+/+}$, *Taok2*$^{+/-}$, and *Taok2*$^{-/-}$ mice with a vibratome in a cutting solution containing 85 mM NaCl, 75 mM sucrose, 2.5 mM KCl, 25 mM glucose, 1.25 mM NaH_2PO_4, 4 mM $MgCl_2$, 0.5 mM $CaCl_2$, and 24 mM $NaHCO_3$ at low temperature. Slices were recovered at 32°C in an incubation chamber with the cutting solution for 30 min followed by another 30 min with perfused oxygenated artificial cerebrospinal fluid (ACSF) containing 127 mM NaCl, 25 mM $NaHCO_3$, 25 mM D-glucose, 1.25 mm NaH_2PO_4, 2.5 mM KCl, 1 mM $MgCl_2$, and 2 mM $CaCl_2$ at pH 7.4, before the treatment. Slices were then treated with puromycin (10 μg/ml) for 90 min to label the newly synthesized proteins. The incubation medium with puromycin was removed followed by two successive washes with oxygenated ACSF for 10 min each before lysis for WB processing or fixation for IHC investigations. To verify the detected signal of the newly synthesized protein by anti-puromycin antibody and whether it is protein synthesis dependent, slices from WT animals were pretreated with CHX (a translation inhibitor, 100 μm/ml) for 30 min before puromycin treatment.

Primary cortical neurons (7DIV or 21DIV), N2a cells (control cells transfected with pcDNA3.1-myc-tag or cells transfected with TAOK2β or TAOK2βA135P or TAOK2α or TAOK2αA135P plasmids), and 5×10^6 LCLs were treated with puromycin (10 μg/ml) in a prewarmed medium and incubated for 10 min at 37°C, 5% CO_2. To verify the detected signal of the newly synthesized protein by anti-puromycin antibody, cells were pretreated with CHX (50 μg/ml) for 5 min at 37°C, 5% CO_2, and then followed by puromycin treatment. After puromycin treatment, the cells were rinsed quickly with a standard medium. Afterward, cells were either fixed for immunostaining or washed twice with ice-cold 1× PBS, pelleted by centrifugation at 1,000 rpm for 5 min at 4°C, and processed with WB for SUnSET analysis.

Immunofluorescence SUnSET analysis

Acute brain slices were fixed with 4% paraformaldehyde (PFA) in PBS for 1.5 hours at RT. Slices were permeabilized with 0.3% Triton X-100 in PBS, followed by incubation in blocking buffer [5% donkey serum in tris-buffered saline (TBS) and 0.5% Triton X-100] for 1.5 hours at RT. Primary antibody incubations were conducted for 48 hours at RT with gentle shaking. After three washes with 1× PBS, slices were incubated with anti–Alexa Fluor–conjugated secondary antibodies in 1× PBS with 0.3% Triton X-100 for 2 hours at RT. Slices were washed three times in 1× PBS and incubated with DAPI for 30 min at RT. Slices were washed three times with 1× PBS and then mounted using a mixture of Mowiol and DABCO. Neurons or N2a cells were fixed with 4% PFA in PBS containing 4% sucrose for 10 min at RT followed by three washes with 1× PBS. Cells were permeabilized with 1× PBS containing 0.3% Triton X-100 and incubated in blocking buffer (5% donkey serum in TBS and 0.3% Triton) for 1.5 hours at RT. Primary antibody incubations were carried out overnight at 4°C, and secondary antibodies were added for 2 hours at RT. After washing, coverslips were stained with DAPI and mounted on glass microscope slides using Fluoromount-G (Southern Biotech).

Slices were imaged by Zeiss LSM 900 confocal laser microscope equipped with Plan-Apochromat 20×/0.8 objective. Z-series images were acquired with a step size of 1 μm in between *z* sections. Cells were imaged by a Nikon microscope (Eclipse, Ti) using an inverted 60× oil immersion objective (numerical aperture, 1.4). Cells were identified by their morphology or immunolabeling by anti–β-tubulin III, anti-TAOK2β or anti–Myc-tag antibodies, or fluorescent markers (tDimer or EGFP). Z-series images were acquired with a step size of 0.3 μm in between z sections. Image acquisition settings were maintained similarly within the experiment. The brightness and contrast of the images were adjusted with the same setting using Photoshop CS 8.0 (Adobe Systems) or ImageJ.

All *z* sections for the entire cell were summed together with the maximum intensity using the z project tool in ImageJ. Afterward, mean puromycin fluorescent intensity in the cell body was measured in randomly selected labeled cells by ImageJ. Only individual cells with no adjacent cells were analyzed to avoid false-positive signals from the other cells. Transfected neurons expressing tDimer and TAOK2β and the nearby nontransfected neurons from one coverslip were selected and processed in parallel to control the conditions. Only N2a cells expressing Myc-tag plus GFP signals were analyzed.

WB SUnSET analysis

Microdissected cortices from the acute slices or N2a cells growing on a 10-cm culture dish or 5×10^6 LCLs following the puromycin treatment were lysed in sterile-filtered radioimmunoprecipitation assay (RIPA) buffer [50 mM tris-HCl (pH 7.4), 150 mM NaCl, 1 mM EGTA, 1% NP-40, and 0.25% sodium deoxycholate (SDC)] supplemented with 1× cOmplete protease inhibitor cocktail (Roche) by sonication 5× every 10 s. The lysates were cleared by centrifugation at 20,000*g* for 10 min at 4°C. Equal amounts of protein were resolved on 10% SDS–polyacrylamide gel electrophoresis (SDS-PAGE) and immunoblotted against puromycin and β-actin. Puromycin protein signal in the whole lane was normalized against β-actin to calculate the puromycin/β-actin ratio using ImageJ. Revert 700 Total Protein Stain for Western Blot Normalization (Licor) was used to show the equal protein loading.

IP using TAOK2β antibody

The cortex of *Taok2*$^{+/+}$ mouse or N2a cells 48 hours after transfection with WT TAOK2β was lysed in ice-cold lysis RIPA buffer (pH 8.2) containing 1× cOmplete protease inhibitor cocktail (Roche). The cellular homogenates were cleared from the cell debris by centrifugation at 13,000 rpm for 10 min at 4°C. Cleared homogenate (1000 μg) was incubated with polyclonal rabbit anti-Taok2β or polyclonal rabbit anti-IgG antibodies prebound to Dynabeads Protein A (Invitrogen) undergoing rotation (25 rpm) overnight at 4°C. The supernatant was removed using a magnetic holder, and the immunoprecipitated complexes were washed three times with a precooled lysis buffer at 4°C. Following another three washes with tris-HCl (pH 8.2) at 4°C, the immunoprecipitated complex was analyzed by LC-MS/MS. For analysis of the immunoprecipitated complex from the cytoplasmic lysates of N2a cells by SDS-PAGE, 50 μl of Laemmli sample buffer was added to the immunoprecipitated complex and boiled for 10 min at 95°C in a heat block to elute the proteins. Afterward, the eluted proteins were loaded on 7.5 to 20% SDS-polyacrylamide gel and processed with the routine WB analysis and immunodetection using anti-Taok2β and anti-eEF2 antibodies.

Neuronal proximity–based proteomic system

To identify PPI in DIV18 neuron, we followed our previously described protocol (*74*).

TCA protein extraction from polysome fractions for WB analysis

Every two to three sucrose fractions were pooled together as indicated in the scheme (Fig. 2, A and B). An equal volume of 20% trichloroacetic acid (TCA) was added to the sample in a microcentrifuge tube and incubated for 30 min on ice. Afterward, the tubes were centrifuged at 14,000 rpm for 5 min. The supernatant was gently removed, and the pellet was washed with 500 μl of cold acetone and spun down at 14,000 rpm for 5 min. After two-acetone washes, the pellets were dried by placing the tubes in a 50°C heating block for 5 min. All procedures were performed under a safety hood. For SDS-PAGE, 50 μl of 2× Laemmli sample buffer was added to each pellet. The pellets of the first three pooled fractions were dissolved in 150 μl of 2× Laemmli sample buffer. The sample was boiled for 10 min at 95°C in a heat block, and 30 μl was loaded onto 10% SDS-PAGE gel for routine WB.

In vitro kinase assay

Either ascending concentrations of 25, 50, 100, and 150 ng of recombinant human protein TAOK2 (amino acids 1 to 314) expressed by baculovirus in Sf9 insect cells using N-terminal GST tag (Signal-Chem, T25-11G-10), or 150 ng of TAOK2 protein (amino acids 1 to 314) containing 60 μm of TAOK2 inhibitor compound 43 (Cp 43) (Tocris, 6558) or equivalent concentration of vehicle dimethyl sulfoxide (DMSO), or 250 ng of TAOK2, recombinant protein 1-314 with mutation A135P, expressed by baculovirus in Sf9 insect cells using N-terminal GST tag (Origene, SR248141; custom made), or its control TAOK2 (amino acids 1 to 314) was incubated with 300 ng of recombinant human protein eEF2 with N-terminal 6× His-tag (MyBioSource, MBS1213669) or recombinant human protein eEF2 with mutation in T56A expressed in *Escherichia coli* with N-terminal 6× His-tag (Origene, SR248140; custom made) in a 25-μl kinase assay buffer I (Signal-Chem, K01-09) supplemented with cOmplete protease inhibitor cocktail (Roche) and phosSTOP (Roche). For control, 300 ng of the recombinant human protein eEF2 protein was incubated in the reaction buffer without adding the recombinant human protein TAOK2 or 150 ng of TAOK2 protein without the eEF2 protein. The kinase reaction was initiated by adding adenosine triphosphate (ATP) to a final concentration of 350 μM and incubation at 30°C for 45 min. In the control reaction, 150 ng of TAOK2 was used under the same reaction conditions without the substrate. The reaction was terminated by adding Laemmli sample buffer and subjected to WB analysis to detect the phosphorylation of eEF2 at its Thr^{56} residue by using an anti–phospho-Thr^{56}–specific rabbit antibody.

Immunoblot

Thirty microliters of sample with Laemmli buffer after TCA protein precipitation from each polysome fraction or 30 to 50 μg of protein determined by Pierce BCA Protein Assay Kit according to the manufacturer's guidelines from cellular or brain lysates were subjected to standard SDS-PAGE. Immunoblotting to polyvinylidene difluoride membrane was performed with the standard wet transfer method. Blots were probed with primary antibodies following the antibody's datasheet instructions. The signals were visualized by HRP-conjugated anti-IgG secondary antibodies, imaged by enhanced chemiluminescence NTAS, ChemoStar, ECL Imager, and analyzed using software from Fiji Software. Proteins of interest were normalized to the β-actin signal, and the phospho-specific signals were normalized to their respective total protein intensity after membrane stripping and redevelopment.

Coomassie stain

One microgram of WT TAOK2 (1 to 314 amino acids) and TAOK2 A135P (amino acids 1 to 314) and 1.5 μg of WT eEF2 and eEF2 (T56A) recombinant proteins were resolved on SDS-PAGE. Following electrophoresis, the protein bands were visualized by quick Coomassie stain (Biozol, ANA-GEN-QC-STAIN-30-ML).

Protein purification from polysomes to detect Taok2 isoforms by proteome analysis

Sucrose polysome fractions 11 to 22 (that represent light and heavy polysomes in the polysome profile) from *Taok2*$^{+/+}$ mouse cortex were collected and pooled together. The proteins were purified from the sucrose and concentrated up to 200 μl final volume by several

washes with ddH_2O using Amicon Ultra-15 centrifugation filter (Millipore) at 4°C. Protein concentration in the sample was determined, and equal amounts of protein were loaded into 10% SDS-PAGE gel. Following electrophoresis, the protein bands were visualized by Coomassie (Roti-Blue) staining solution (Roth) for 30 min at RT. The gel was washed several times with 25% methanol solution until the bands were visible. The bands at approximate 100 to 160 kDa corresponding to Taok2 molecular weight were excised, digested, and analyzed by LC-MS/MS.

Proteome analysis for the purified protein from polysomes and the immunoprecipitated proteins with LC-MS/MS

Tryptic in-gel digestion was conducted following a previously described protocol (*77*). Shrinking and swelling of gel pieces were performed with 100% acetonitrile (ACN) and 100 mM ammonium bicarbonate (NH_4HCO_3). The in-gel reduction was conducted with 10 mM DTT (dissolved in 100 mM NH_4HCO_3). Alkylation was performed at RT with 55 mM iodoacetamide (dissolved in 100 mMNH_4HCO_3). Digestion of proteins in the gel pieces was done by covering them with a trypsin solution containing sequencing-grade trypsin (8 ng/μl; Promega), dissolved in 50 mM NH_4HCO_3 with 10% ACN. The mixture was incubated overnight at 37°C. Tryptic peptide products were further yielded by extraction with 2% formic acid (FA) and 80% ACN. The extract was evaporated. For LC-MS/MS analysis, samples were resuspended in 20 μl of 0.1% FA. Protein digestion of the immunoprecipitated samples was performed on the magnetic beads. Therefore, 1% SDC in 100 mM triethylammonium bicarbonate was added and the samples were boiled at 95°C for 5 min. DTT was added to the sample (final concentration, 10 mM) and incubated at 60°C for 30 min. Iodoacetamide was added to the samples (final concentration, 20 mM) and incubated at 37°C for 30 min. Proteins were digested with trypsin (sequencing grade, Promega) at 37°C overnight. After digestion, samples were placed on a magnetic rack and left for 1 min to settle, the supernatant was transferred to a new tube, and 1% FA was added to stop digestion and precipitate SDC. Samples were then centrifuged at 16,000*g* for 5 min, and the supernatant was transferred to a new tube and dried in a vacuum centrifuge.

Samples were reconstituted in 0.1% FA and transferred into a full recovery autosampler vial (Waters). Chromatographic separation was achieved on a Dionex Ultimate 3000 UPLC system (Thermo Fisher Scientific) with a two-buffer system (buffer A: 0.1% FA in water; buffer B: 0.1% FA in ACN). Attached to the UPLC was an Acclaim PepMap 100 C18 trap (100 μm by 2 cm, 100-Å pore size, 5-μm particle size, Thermo Fisher Scientific) for desalting a purification followed by a nanoEase M/Z peptide BEH130 C18 column (75 μm by 25 cm, 130-Å pore size, 1.7-μm particle size, Waters). Peptides were separated using a 60-min gradient with increasing ACN concentration from 2 to 30% ACN. The eluted peptides were analyzed on a quadrupole orbitrap ion trap tribrid mass spectrometer (Fusion, Thermo Fisher Scientific) in data-dependent acquisition (DDA). The fusion was operated at top speed mode analyzing the most intense ions per precursor scan (2×10^5 ions, 120,000 resolution, 120-ms fill time) within 3 s and was analyzed by MS/MS in the ion trap [Higher-energy collisional dissociation (HCD) at 30 normalized collision energy (NCE), 1×10^4 ions, 60-ms fill time] in a range of 400 to 1300 mass/charge ratio (m/z). A dynamic precursor exclusion with a speed mode of 20 s was used.

The acquired DDA LC-MS/MS data were searched against the UniProt mouse protein database (release October 2020, 17,053 protein entries) and the TAOK2 splice variant 2 (Q6ZQ29-2) using the Sequest algorithm integrated into the Proteome Discoverer software version 2.4 in label-free quantification mode. The match between runs was enabled, and performing chromatographic retention recalibration for precursors with a 5-min retention time tolerance, no scaling, and no normalization for extracted peptide areas was done. The following parameters were applied in the searches: Mass tolerances for precursors were set to 10 parts per million (ppm), and fragment mass tolerance was 0.6 Da. Carbamidomethylation was set as a fixed modification for cysteine residues, and the oxidation of methionine, pyro-glutamate formation at glutamine residues at the peptide N terminus, as well as acetylation of the protein N terminus, loss of methionine at the protein N terminus, and the acetylation after methionine loss at the protein N terminus were permitted as variable modifications for the search. Peptide areas were summed to protein areas and used for quantitative analysis. Only the peptides with high confidence [false discovery rate (FDR) < 1% using a decoy database approach] were accepted as identified. Peptide areas were summed to protein areas and used for quantitative analysis. Protein areas were imported into Perseus software version 1.5.8 for statistical analysis.

N2a cells and mouse cortices were run in duplicates with their corresponding IgG controls. The resulting protein abundance was first averaged between the respective samples, and only proteins with a nonzero count in at least one of the duplicates in the IgG control were kept for further analysis in R with customs scripts (v. 4.1.0, available at https://github.com/TabithaRuecker/TaoK2beta). The filtered protein abundances comprised 293 proteins for N2a cells and 194 proteins for the cortex. In the parallel PPI analysis from cultured neurons, we performed a *t* test for further confidence of protein detection with a *P* value of 0.05 and a positive fold change compared to the luciferase control as cutoff, resulting in identified 150 proteins in neuronal cell culture for 18DIV. The ORA depiction as cnetplot between the three MS approaches (N2a cells overexpressing TaoK2β, cortex, and DIV18 neurons) was generated using enrichplot R package v. 1.12.3. The dotplot was generated by applying compare Cluster function from R package clusterProfiler v. 4.0.5 with a *P* value cutoff of 1 and enrich GO parameter.

Total proteomics and phosphoproteomics of *Taok2*$^{-/-}$ mouse brain regions

Frozen tissue was punched from 1-mm slices from the prefrontal cortex, ventral striatum, and hippocampus of P21 *Taok2* +/+ (6), *Taok2* +/− (5), or *Taok2* −/− (5) mouse brain. Tissue was lysed for 30 min on ice in lysis buffer containing 8 M urea, 50 mM Hepes, pH 8.0, 1 mM DTT, cOmplete protease inhibitor cocktail (Roche), and phosSTOP (Roche) followed by 3× 10-s sonication. Protein (100 μg) was reduced with 5 mM DTT for 30 min at 37°C and alkylated with 15 mM iodoacetamide for 30 min at RT in the dark. Proteins were digested with 4 μg of trypsin/Lys-C mix (Promega, V5073) for 3 to 4 hours at 37°C, diluted 4× with 50 mM Hepes (pH 8.0) to reactivate trypsin, and incubated overnight at 37°C. Samples were desalted using Pierce Peptide Desalting Columns (Thermo Fisher Scientific, 89851) and vacuum-dried completely. Dried peptides were dissolved in Hepes (pH 8.5) and labeled with 0.5 mg of TMTpro 16plex Isobaric Label Reagent Set (Thermo Fisher Scientific, A44522). Individually labeled samples were combined and desalted using a Pierce Peptide Desalting Column (Thermo Fisher Scientific, 89851). Labeled peptides were dried and used for sequential enrichment

with metal oxide affinity chromatography. First, phosphopeptides were enriched using High-Select TiO_2 Phosphopeptide Enrichment Kit (Thermo Fisher Scientific, A32993). The flowthrough was subsequently enriched using the High-Select Fe-NTA Phosphopeptide Enrichment Kit (Thermo Fisher Scientific, A32992). Elutions of both steps were combined and used for phosphoproteomics MS. The final flowthrough was used for total proteomics MS.

Fifty micrograms of dried peptides was redissolved in 100 µl of solvent A [10 mM ammonium bicarbonate in water/ACN (98:2, v/v), pH 5.5]. Fractionation was performed by reversed-phase high-performance LC (Agilent series 1200) connected to a Probot fractionator (LC Packings), where 95 µl was loaded onto a 4-cm precolumn [made in-house, 250-µm internal diameter (ID), 5-µm C18 beads, Dr. Maisch] for 10 min followed by separation on a 15-cm analytical column (made in-house, 250-µm ID, 3-µm C18 beads, Dr. Maisch) with a linear gradient from 0% solvent B [10 mM ammonium bicarbonate in water/ACN (30:70, v/v), pH 5.5] up to 100% solvent B in 120 min at a flow rate of 3 µl/min. One-minute fractions were pooled every 12 min into 12 pooled fractions, vacuum-dried, and stored at −20°C until LC-MS/MS analysis.

Each fraction was solubilized in 30 µl of loading solvent A [0.1% trifluoroacetic acid in water:ACN (98:2, v/v)] moments before analysis, and 12/13 µl was injected for LC-MS/MS analysis on an Ultimate 3000 RSLCnano system in-line connected to an Orbitrap Fusion Lumos mass spectrometer (Thermo Fisher Scientific). Trapping was performed at 10 µl/min for 4 min in loading solvent A on a 20-mm trapping column (made in-house, 100-µm ID, 5-µm beads, C18 Reprosil-HD, Dr. Maisch, Germany). The peptides were separated on a 200-cm µPAC column (C18-endcapped functionality, 300-µm-wide channels, 5-µm porous-shell pillars, interpillar distance of 2.5 µm, and a depth of 20 µm; Pharmafluidics, Belgium). It was kept at a constant temperature of 50°C. Peptides were eluted by a linear gradient reaching 55% MS solvent B [0.1% FA in water/ACN (2:8, v/v)] after 85 min and 99% MS solvent B at 90 min, followed by a 10-min wash at 99% MS solvent B and reequilibration with MS solvent A (0.1% FA in water). For the first 15 min, the flow rate was set to 750 nl/min, after which it was kept constant at 300 nl/min.

Total proteomics was performed using an SPS-MS3 method, with the mass spectrometer operated in data-dependent mode with a top speed of 3 s. Full-scan MS spectra (375 to 1500 m/z) were acquired at a resolution of 120,000 in the Orbitrap analyzer after accumulation to a target automatic gain control (AGC) value of 400,000 with a maximum injection time of 50 ms. The precursor ions were filtered for charge states (two to seven required), dynamic exclusion (60 s; ±10-ppm window), and intensity (minimal intensity of 5×10^4). The precursor ions were selected in the quadrupole with an isolation window of 0.7 Da and accumulated to an AGC target of 1×10^4 or a maximum injection time of 50 ms and activated using collision-induced dissociation fragmentation (35% NCE). The fragments were analyzed in the ion trap analyzer at a turbo scan rate. The 10 most intense MS2 fragments were selected in the quadrupole using MS3 multi-notch isolation windows of 3 m/z. An orbitrap resolution of 60,000 was used with an AGC target of 1×10^5 or a maximum injection time of 118 ms and activated using HCD fragmentation (65% NCE).

Phosphoproteomics was performed like the total proteomics samples but instead using an SPS-MS3 with a multistage activation method. The fragments were analyzed in the Orbitrap Analyzer with a resolution of 30,000. The 10 most intense MS2 fragments were selected in the quadrupole using MS3 multi-notch isolation windows of 3 m/z. An orbitrap resolution of 60,000 was used with an AGC target of 1×10^5 or a maximum injection time of 105 ms and activated using HCD fragmentation (65% NCE).

Database search was done with the MaxQuant software (v 1.6.2.6) using the Andromeda search engine with the default search settings including an FDR set at 1% on both the peptide and protein level. Reporter ion MS3 was set as search type, and TMT16pro isobaric labels were manually entered with appropriate correction factors. Reporter mass tolerance was set at 0.003 Da. Spectra were searched against the *Mus musculus* database of UniProt (August 2020) and the common contaminant list provided by the software. The MS1 mass tolerance for the first search and the main search was set to 20 and 4.5 ppm, respectively. The MS2 match tolerance is set at 20 ppm. Enzyme specificity was set to trypsin/P with digestion at the C-terminal of Arg and Lys residues, even when they were followed by a Pro residue, with a maximum of two missed cleavages. Variable modifications were set to oxidation (Met) and protein N-terminal acetylation. Carbamidomethylation of Cys residues was set as a fixed modification. For phosphoproteomics, phosphorylation at serine, threonine, or tyrosine residues was set as a variable modification. A minimum of one peptide (razor or unique) was required for identification with a minimum length of seven residues. Second peptide search was allowed as well as the matching between runs option (from and to) using a 0.7-min match time window and 20-min alignment window.

Data were further processed in Perseus v.1.6.15.0. Protein groups and phospho (STY) sites from the MaxQuant search were loaded, and site tables were expanded. Potential contaminants, reversed hits and proteins that were identified only by site, were removed. Reporter intensities were $\log_2$-transformed and filtered for rows containing only valid values. Columns were normalized by subtracting the median. Potential TAOK2 substrates were annotated using the pT-X-X-[RKH] motif. A multi-scatter plot and principal components analysis were calculated to determine the quality of the runs. A two-sample t test was performed comparing the WT and knockout conditions with a permutation-based FDR of 0.05 and an S0 value of 0.1 for truncation with a total of 250 randomizations.

GSEA was performed on the total proteomics dataset ranked by signed log-transformed P values using the Molecular Signatures Database GO Biological Process collection (MsigDB, v7.5.1). The preranked list was given as input to GSEAPreranked (v4.2.2) with default parameters. Network analysis was done with EnrichmentMap and AutoAnnotate in Cytoscape (v3.9.1) using an FDR cutoff of 0.1 and similarity cutoff of 0.375.

The MS proteomics data have been deposited to the ProteomeXchange Consortium via the PRIDE (*78*) partner repository with the dataset identifier PXD03837.

Proteomic analysis for the TAOK2 and eEF2 recombinant human proteins

One microgram from the recombinant human protein TAOK2 (amino acids 1 to 314) (Signal-Chem, T25-11G-10) or the recombinant human protein eEF2 (MyBioSource, MBS1213669) was subjected to process of denaturation, reduction, alkylation, and digestion and processed for normal proteomics as mentioned previously. The detected peptides were aligned with the human proteome, with the *Spodoptera frugiperda* proteome, and a contaminants database.

Statistical analysis

The GraphPad Prism (version 10) analytic software was used to perform all the statistical analyses. Several biological replicates, experiments, and statistical tests used for the comparison were mentioned within the figure legends and in tables S6 and S7.

Supplementary Materials

This PDF file includes:

Figs. S1 to S10
Legends for tables S1 to S7

Other Supplementary Material for this manuscript includes the following:

Tables S1 to S7

REFERENCES AND NOTES

1. Y. Liu, A. Beyer, R. Aebersold, On the dependency of cellular protein levels on mRNA abundance. *Cell* **165**, 535–550 (2016).
2. M. L. Truitt, D. Ruggero, New frontiers in translational control of the cancer genome. *Nat. Rev. Cancer* **17**, 332 (2017).
3. C. G. Proud, Phosphorylation and signal transduction pathways in translational control. *Cold Spring Harb. Perspect. Biol.* **11**, a033050 (2019).
4. A. G. Hinnebusch, J. R. Lorsch, The mechanism of eukaryotic translation initiation: New insights and challenges. *Cold Spring Harb. Perspect. Biol.* **4**, a011544 (2012).
5. X. M. Ma, J. Blenis, Molecular mechanisms of mTOR-mediated translational control. *Nat. Rev. Mol. Cell Biol.* **10**, 307–318 (2009).
6. N. Sonenberg, A. G. Hinnebusch, Regulation of translation initiation in eukaryotes: Mechanisms and biological targets. *Cell* **136**, 731–745 (2009).
7. T. E. Dever, L. Feng, R. C. Wek, A. M. Cigan, T. F. Donahue, A. G. Hinnebusch, Phosphorylation of initiation factor 2α by protein kinase GCN2 mediates gene-specific translational control of GCN4 in yeast. *Cell* **68**, 585–596 (1992).
8. M. Costa-Mattioli, D. Gobert, E. Stern, K. Gamache, R. Colina, C. Cuello, W. Sossin, R. Kaufman, J. Pelletier, K. Rosenblum, K. Krnjevic, J. C. Lacaille, K. Nader, N. Sonenberg, eIF2α phosphorylation bidirectionally regulates the switch from short- to long-term synaptic plasticity and memory. *Cell* **129**, 195–206 (2007).
9. M. Costa-Mattioli, P. Walter, The integrated stress response: From mechanism to disease. *Science* **368**, eaat5314 (2020).
10. A. G. Ryazanov, E. A. Shestakova, P. G. Natapov, Phosphorylation of elongation factor 2 by EF-2 kinase affects rate of translation. *Nature* **334**, 170–173 (1988).
11. N. T. Redpath, C. G. Proud, Purification and phosphorylation of elongation factor-2 kinase from rabbit reticulocytes. *Eur. J. Biochem.* **212**, 511–520 (1993).
12. J. W. Kenney, C. E. Moore, X. Wang, C. G. Proud, Eukaryotic elongation factor 2 kinase, an unusual enzyme with multiple roles. *Adv. Biol. Regul.* **55**, 15–27 (2014).
13. D. Kuzuoglu-Ozturk, Z. Hu, M. Rama, E. Devericks, J. Weiss, G. G. Chiang, S. T. Worland, S. E. Brenner, H. Goodarzi, L. A. Gilbert, D. Ruggero, Revealing molecular pathways for cancer cell fitness through a genetic screen of the cancer translatome. *Cell Rep.* **35**, 109321 (2021).
14. M. Kapur, C. E. Monaghan, S. L. Ackerman, Regulation of mRNA translation in neurons—A matter of life and death. *Neuron* **96**, 616–637 (2017).
15. W. S. Sossin, M. Costa-Mattioli, Translational control in the brain in health and disease. *Cold Spring Harb. Perspect. Biol.* **11**, a032912 (2019).
16. M. J. Maenner, K. A. Shaw, J. Baio, A. Washington, M. Patrick, M. D. Rienzo, D. L. Christensen, L. D. Wiggins, S. Pettygrove, J. G. Andrews, M. Lopez, A. Hudson, T. Baroud, Y. Schwenk, T. White, C. R. Rosenberg, L.-C. Lee, R. A. Harrington, M. Huston, A. Hewitt, A. Esler, J. Hall-Lande, J. N. Poynter, L. Hallas-Muchow, J. N. Constantino, R. T. Fitzgerald, W. Zahorodny, J. Shenouda, J. L. Daniels, Z. Warren, A. Vehorn, A. Salinas, M. S. Durkin, P. M. Dietz, Prevalence of autism spectrum disorder among children aged 8 years—Autism and developmental disabilities monitoring network, 11 sites, United States, 2016. *MMWR Surveill. Summ.* **69**, 1–12 (2020).
17. M. K. Belmonte, G. Allen, A. Beckel-Mitchener, L. M. Boulanger, R. A. Carper, S. J. Webb, Autism and abnormal development of brain connectivity. *J. Neurosci.* **24**, 9228–9231 (2004).
18. R. J. Kelleher III, M. F. Bear, The autistic neuron: Troubled translation? *Cell* **135**, 401–406 (2008).
19. E. H. Cook Jr., S. W. Scherer, Copy-number variations associated with neuropsychiatric conditions. *Nature* **455**, 919–923 (2008).
20. S. Steinberg, S. de Jong, M. Mattheisen, J. Costas, D. Demontis, S. Jamain, O. P. H. Pietiläinen, K. Lin, S. Papiol, J. Huttenlocher, E. Sigurdsson, E. Vassos, I. Giegling, R. Breuer, G. Fraser, N. Walker, I. Melle, S. Djurovic, I. Agartz, A. Tuulio-Henriksson, J. Suvisaari, J. Lönnqvist, T. Paunio, L. Olsen, T. Hansen, A. Ingason, M. Pirinen, E. Strengman, GROUP, D. M. Hougaard, T. Orntoft, M. Didriksen, M. V. Hollegaard, M. Nordentoft, L. Abramova, V. Kaleda, M. Arrojo, J. Sanjuán, C. Arango, B. Etain, F. Bellivier, A. Méary, F. Schürhoff, A. Szoke, M. Ribolsi, V. Magni, A. Siracusano, S. Sperling, M. Rossner, C. Christiansen, L. A. Kiemeney, B. Franke, L. H. van den Berg, J. Veldink, S. Curran, P. Bolton, M. Poot, W. Staal, K. Rehnstrom, H. Kilpinen, C. M. Freitag, J. Meyer, P. Magnusson, E. Saemundsen, I. Martsenkovsky, I. Bikshaieva, I. Martsenkovska, O. Vashchenko, M. Raleva, K. Paketchieva, B. Stefanovski, N. Durmishi, M. P. Milovancevic, D. L. Tosevski, T. Silagadze, N. Naneishvili, N. Mikeladze, S. Surguladze, J. B. Vincent, A. Farmer, P. B. Mitchell, A. Wright, P. R. Schofield, J. M. Fullerton, G. W. Montgomery, N. G. Martin, I. A. Rubino, R. van Winkel, G. Kenis, M. De Hert, J. M. Réthelyi, I. Bitter, L. Terenius, E. G. Jönsson, S. Bakker, J. van Os, A. Jablensky, M. Leboyer, E. Bramon, J. Powell, R. Murray, A. Corvin, M. Gill, D. Morris, F. A. O'Neill, K. Kendler, B. Riley, Wellcome Trust Case Control Consortium, N. Craddock, M. J. Owen, M. C. O'Donovan, U. Thorsteinsdottir, A. Kong, H. Ehrenreich, A. Carracedo, V. Golimbet, O. A. Andreassen, A. D. Børglum, O. Mors, P. B. Mortensen, T. Werge, R. A. Ophoff, M. M. Nöthen, M. Rietschel, S. Cichon, M. Ruggeri, S. Tosato, A. Palotie, D. St. Clair, D. Rujescu, D. A. Collier, H. Stefansson, K. Stefansson, Common variant at 16p11.2 conferring risk of psychosis. *Mol. Psychiatry* **19**, 108–114 (2014).
21. L. A. Weiss, Y. Shen, J. M. Korn, D. E. Arking, D. T. Miller, R. Fossdal, E. Saemundsen, H. Stefansson, M. A. Ferreira, T. Green, O. S. Platt, D. M. Ruderfer, C. A. Walsh, D. Altshuler, A. Chakravarti, R. E. Tanzi, K. Stefansson, S. L. Santangelo, J. F. Gusella, P. Sklar, B.-L. Wu, M. J. Daly, Autism Consortium, Association between microdeletion and microduplication at 16p11.2 and autism. *N. Engl. J. Med.* **358**, 667–675 (2008).
22. S. E. McCarthy, V. Makarov, G. Kirov, A. M. Addington, J. M. Clellan, S. Yoon, D. O. Perkins, D. E. Dickel, M. Kusenda, O. Krastoshevsky, V. Krause, R. A. Kumar, D. Grozeva, D. Malhotra, T. Walsh, E. H. Zackai, P. Kaplan, J. Ganesh, I. D. Krantz, N. B. Spinner, P. Roccanova, A. Bhandari, K. Pavon, B. Lakshmi, A. Leotta, J. Kendall, Y.-H. Lee, V. Vacic, S. Gary, L. M. Iakoucheva, T. J. Crow, S. L. Christian, J. A. Lieberman, T. S. Stroup, T. Lehtimäki, K. Puura, C. Haldeman-Englert, J. Pearl, M. Goodell, V. L. Willour, P. Derosse, J. Steele, L. Kassem, J. Wolff, N. Chitkara, F. J. McMahon, A. K. Malhotra, J. B. Potash, T. G. Schulze, M. M. Nöthen, S. Cichon, M. Rietschel, E. Leibenluft, V. Kustanovich, C. M. Lajonchere, J. S. Sutcliffe, D. Skuse, M. Gill, L. Gallagher, N. R. Mendell, Wellcome Trust Case Control Consortium, N. Craddock, M. J. Owen, M. C. O'Donovan, T. H. Shaikh, E. Susser, L. E. Delisi, P. F. Sullivan, C. K. Deutsch, J. Rapoport, D. L. Levy, M.-C. King, J. Sebat, Microduplications of 16p11.2 are associated with schizophrenia. *Nat. Genet.* **41**, 1223–1227 (2009).
23. C. Mitsopoulos, C. Zihni, R. Garg, A. J. Ridley, J. D. H. Morris, The prostate-derived sterile 20-like kinase (PSK) regulates microtubule organization and stability. *J. Biol. Chem.* **278**, 18085–18091 (2003).
24. S. Yasuda, H. Tanaka, H. Sugiura, K. Okamura, T. Sakaguchi, U. Tran, T. Takemiya, A. Mizoguchi, Y. Yagita, T. Sakurai, E. M. De Robertis, K. Yamagata, Activity-induced protocadherin arcadlin regulates dendritic spine number by triggering N-cadherin endocytosis via TAO2beta and p38 MAP kinases. *Neuron* **56**, 456–471 (2007).
25. M. Richter, N. Murtaza, R. Scharrenberg, S. H. White, O. Johanns, S. Walker, R. K. C. Yuen, B. Schwanke, B. Bedurftig, M. Henis, S. Scharf, V. Kraus, R. Dork, J. Hellmann, Z. Lindenmaier, J. Ellegood, H. Hartung, V. Kwan, J. Sedlacik, J. Fiehler, M. Schweizer, J. P. Lerch, I. L. Hanganu-Opatz, F. Morellini, S. W. Scherer, K. K. Singh, F. Calderon de Anda, Altered TAOK2 activity causes autism-related neurodevelopmental and cognitive abnormalities through RhoA signaling. *Mol. Psychiatry* **24**, 1329–1350 (2019).
26. E. Santini, T. N. Huynh, A. F. MacAskill, A. G. Carter, P. Pierre, D. Ruggero, H. Kaphzan, E. Klann, Exaggerated translation causes synaptic and behavioural aberrations associated with autism. *Nature* **493**, 411–415 (2013).
27. R. Scharrenberg, M. Richter, O. Johanns, D. P. Meka, T. Rucker, N. Murtaza, Z. Lindenmaier, J. Ellegood, A. Naumann, B. Zhao, B. Schwanke, J. Sedlacik, J. Fiehler, I. L. Hanganu-Opatz, J. P. Lerch, K. K. Singh, F. C. de Anda, TAOK2 rescues autism-linked developmental deficits in a 16p11.2 microdeletion mouse model. *Mol. Psychiatry* **27**, 4707–4721 (2022).
28. N. Murtaza, A. A. Cheng, C. O. Brown, D. P. Meka, S. Hong, J. A. Uy, J. El-Hajjar, N. Pipko, B. K. Unda, B. Schwanke, S. Xing, B. Thiruvahindrapuram, W. Engchuan, B. Trost, E. Deneault, F. Calderon de Anda, B. W. Doble, J. Ellis, E. Anagnostou, G. D. Bader, S. W. Scherer, Y. Lu, K. K. Singh, Neuron-specific protein network mapping of autism risk genes identifies shared biological mechanisms and disease-relevant pathologies. *Cell Rep.* **41**, 111678 (2022).
29. B. Schwanhausser, D. Busse, N. Li, G. Dittmar, J. Schuchhardt, J. Wolf, W. Chen, M. Selbach, Global quantification of mammalian gene expression control. *Nature* **473**, 337–342 (2011).
30. C. A. Hoeffer, K. K. Cowansage, E. C. Arnold, J. L. Banko, N. J. Moerke, R. Rodriguez, E. K. Schmidt, E. Klosi, M. Chorev, R. E. Lloyd, P. Pierre, G. Wagner, J. E. LeDoux, E. Klann, Inhibition of the interactions between eukaryotic initiation factors 4E and 4G impairs long-term associative memory consolidation but not reconsolidation. *Proc. Natl. Acad. Sci. U.S.A.* **108**, 3383–3388 (2011).
31. E. K. Schmidt, G. Clavarino, M. Ceppi, P. Pierre, SUnSET, a nonradioactive method to monitor protein synthesis. *Nat. Methods* **6**, 275–277 (2009).

32. S. Yadav, J. A. Oses-Prieto, C. J. Peters, J. Zhou, S. J. Pleasure, A. L. Burlingame, L. Y. Jan, Y. N. Jan, TAOK2 kinase mediates PSD95 stability and dendritic spine maturation through septin7 phosphorylation. *Neuron* **93**, 379–393 (2017).
33. A. P. Schuller, R. Green, Roadblocks and resolutions in eukaryotic translation. *Nat. Rev. Mol. Cell Biol.* **19**, 526–541 (2018).
34. S. Park, J. M. Park, S. Kim, J. A. Kim, J. D. Shepherd, C. L. Smith-Hicks, S. Chowdhury, W. Kaufmann, D. Kuhl, A. G. Ryazanov, R. L. Huganir, D. J. Linden, P. F. Worley, Elongation factor 2 and fragile X mental retardation protein control the dynamic translation of Arc/Arg3.1 essential for mGluR-LTD. *Neuron* **59**, 70–83 (2008).
35. C. Y. Koo, C. Giacomini, M. Reyes-Corral, Y. Olmos, I. A. Tavares, C. M. Marson, S. Linardopoulos, A. N. Tutt, J. D. H. Morris, Targeting TAO kinases using a new inhibitor compound delays mitosis and induces mitotic cell death in centrosome amplified breast cancer cells. *Mol. Cancer Ther.* **16**, 2410–2421 (2017).
36. U. Carlberg, A. Nilsson, O. Nygard, Functional properties of phosphorylated elongation factor 2. *Eur. J. Biochem.* **191**, 639–645 (1990).
37. G. Horev, J. Ellegood, J. P. Lerch, Y.-E. Son, L. Muthuswamy, H. Vogel, A. M. Krieger, A. Buja, R. M. Henkelman, M. Wigler, A. A. Mills, Dosage-dependent phenotypes in models of 16p11.2 lesions found in autism. *Proc. Natl. Acad. Sci. U.S.A.* **108**, 17076–17081 (2011).
38. J. W. B. Hershey, N. Sonenberg, M. B. Mathews, Principles of translational control. *Cold Spring Harb. Perspect. Biol.* **11**, a032607 (2019).
39. Y. C. Chen, Y. W. Chang, Y. S. Huang, Dysregulated translation in neurodevelopmental disorders: An overview of autism-risk genes involved in translation. *Dev. Neurobiol.* **79**, 60–74 (2019).
40. F. Zalfa, M. Giorgi, B. Primerano, A. Moro, A. Di Penta, S. Reis, B. Oostra, C. Bagni, The fragile X syndrome protein FMRP associates with BC1 RNA and regulates the translation of specific mRNAs at synapses. *Cell* **112**, 317–327 (2003).
41. L. de la Torre-Ubieta, H. Won, J. L. Stein, D. H. Geschwind, Advancing the understanding of autism disease mechanisms through genetics. *Nat. Med.* **22**, 345–361 (2016).
42. S. De Rubeis, X. He, A. P. Goldberg, C. S. Poultney, K. Samocha, A. E. Cicek, Y. Kou, L. Liu, M. Fromer, S. Walker, T. Singh, L. Klei, J. Kosmicki, F. Shih-Chen, B. Aleksic, M. Biscaldi, P. F. Bolton, J. M. Brownfeld, J. Cai, N. G. Campbell, A. Carracedo, M. H. Chahrour, A. G. Chiocchetti, H. Coon, E. L. Crawford, S. R. Curran, G. Dawson, E. Duketis, B. A. Fernandez, L. Gallagher, E. Geller, S. J. Guter, R. S. Hill, J. Ionita-Laza, P. J. Gonzalez, H. Kilpinen, S. M. Klauck, A. Kolevzon, I. Lee, I. Lei, J. Lei, T. Lehtimäki, C.-F. Lin, A. Ma'ayan, C. R. Marshall, A. L. McInnes, B. Neale, M. J. Owen, N. Ozaki, M. Parellada, J. R. Parr, S. Purcell, K. Puura, D. Rajagopalan, K. Rehnström, A. Reichenberg, A. Sabo, M. Sachse, S. J. Sanders, C. Schafer, M. Schulte-Rüther, D. Skuse, C. Stevens, P. Szatmari, K. Tammimies, O. Valladares, A. Voran, W. Li-San, L. A. Weiss, A. J. Willsey, T. W. Yu, R. K. C. Yuen, DDD Study, Homozygosity Mapping Collaborative for Autism, UK10K Consortium, E. H. Cook, C. M. Freitag, M. Gill, C. M. Hultman, T. Lehner, A. Palotie, G. D. Schellenberg, P. Sklar, M. W. State, J. S. Sutcliffe, C. A. Walsh, S. W. Scherer, M. E. Zwick, J. C. Barett, D. J. Cutler, K. Roeder, B. Devlin, M. J. Daly, J. D. Buxbaum, Synaptic, transcriptional and chromatin genes disrupted in autism. *Nature* **515**, 209–215 (2014).
43. C. G. Gkogkas, A. Khoutorsky, I. Ran, E. Rampakakis, T. Nevarko, D. B. Weatherill, C. Vasuta, S. Yee, M. Truitt, P. Dallaire, F. Major, P. Lasko, D. Ruggero, K. Nader, J. C. Lacaille, N. Sonenberg, Autism-related deficits via dysregulated eIF4E-dependent translational control. *Nature* **493**, 371–377 (2013).
44. E. Santini, T. N. Huynh, F. Longo, S. Y. Koo, E. Mojica, L. D'Andrea, C. Bagni, E. Klann, Reducing eIF4E-eIF4G interactions restores the balance between protein synthesis and actin dynamics in fragile X syndrome model mice. *Sci. Signal.* **10**, eaan0665 (2017).
45. S. K. Ultanir, S. Yadav, N. T. Hertz, J. A. Oses-Prieto, S. Claxton, A. L. Burlingame, K. M. Shokat, L. Y. Jan, Y. N. Jan, MST3 kinase phosphorylates TAO1/2 to enable Myosin Va function in promoting spine synapse development. *Neuron* **84**, 968–982 (2014).
46. F. L. Pennemann, A. Mussabekova, C. Urban, A. Stukalov, L. L. Andersen, V. Grass, T. M. Lavacca, C. Holze, L. Oubraham, Y. Benamrouche, E. Girardi, R. E. Boulos, R. Hartmann, G. Superti-Furga, M. Habjan, J. L. Imler, C. Meignin, A. Pichlmair, Cross-species analysis of viral nucleic acid interacting proteins identifies TAOKs as innate immune regulators. *Nat. Commun.* **12**, 7009 (2021).
47. A. Castello, B. Fischer, K. Eichelbaum, R. Horos, B. M. Beckmann, C. Strein, N. E. Davey, D. T. Humphreys, T. Preiss, L. M. Steinmetz, J. Krijgsveld, M. W. Hentze, Insights into RNA biology from an atlas of mammalian mRNA-binding proteins. *Cell* **149**, 1393–1406 (2012).
48. M. Caudron-Herger, S. F. Rusin, M. E. Adamo, J. Seiler, V. K. Schmid, E. Barreau, A. N. Kettenbach, S. Diederichs, R-DeeP: Proteome-wide and quantitative identification of RNA-dependent proteins by density gradient ultracentrifugation. *Mol. Cell* **75**, 184–199. e10 (2019).
49. M. R. Santoro, S. M. Bray, S. T. Warren, Molecular mechanisms of fragile X syndrome: A twenty-year perspective. *Annu. Rev. Pathol.* **7**, 219–245 (2012).
50. C. A. Hoeffer, E. Sanchez, R. J. Hagerman, Y. Mu, D. V. Nguyen, H. Wong, A. M. Whelan, R. S. Zukin, E. Klann, F. Tassone, Altered mTOR signaling and enhanced CYFIP2 expression levels in subjects with fragile X syndrome. *Genes Brain Behav.* **11**, 332–341 (2012).
51. J. Zhou, L. F. Parada, PTEN signaling in autism spectrum disorders. *Curr. Opin. Neurobiol.* **22**, 873–879 (2012).
52. S. S. Jeste, M. Sahin, P. Bolton, G. B. Ploubidis, A. Humphrey, Characterization of autism in young children with tuberous sclerosis complex. *J. Child Neurol.* **23**, 520–525 (2008).
53. C. Gross, G. J. Bassell, Excess protein synthesis in FXS patient lymphoblastoid cells can be rescued with a p110β-selective inhibitor. *Mol. Med.* **18**, 336–345 (2012).
54. S. Jacquemont, L. Pacini, A. E. Jonch, G. Cencelli, I. Rozenberg, Y. He, L. D'Andrea, G. Pedini, M. Eldeeb, R. Willemsen, F. Gasparini, F. Tassone, R. Hagerman, B. Gomez-Mancilla, C. Bagni, Protein synthesis levels are increased in a subset of individuals with fragile X syndrome. *Hum. Mol. Genet.* **27**, 2039–2051 (2018).
55. N. Raj, Z. T. McEachin, W. Harousseau, Y. Zhou, F. Zhang, M. E. Merritt-Garza, J. M. Taliaferro, M. Kalinowska, S. G. Marro, C. M. Hales, E. Berry-Kravis, M. W. Wolf-Ochoa, V. Martinez-Cerdeno, M. Wernig, L. Chen, E. Klann, S. T. Warren, P. Jin, Z. Wen, G. J. Bassell, Cell-type-specific profiling of human cellular models of fragile X syndrome reveal PI3K-dependent defects in translation and neurogenesis. *Cell Rep.* **35**, 108991 (2021).
56. Z. Chen, M. H. Cobb, Regulation of stress-responsive mitogen-activated protein (MAP) kinase pathways by TAO2. *J. Biol. Chem.* **276**, 16070–16075 (2001).
57. Z. Chen, M. Hutchison, M. H. Cobb, Isolation of the protein kinase TAO2 and identification of its mitogen-activated protein kinase/extracellular signal-regulated kinase kinase binding domain. *J. Biol. Chem.* **274**, 28803–28807 (1999).
58. M. Costa-Mattioli, D. Gobert, H. Harding, B. Herdy, M. Azzi, M. Bruno, M. Bidinosti, C. Ben Mamou, E. Marcinkiewicz, M. Yoshida, H. Imataka, A. C. Cuello, N. Seidah, W. Sossin, J. C. Lacaille, D. Ron, K. Nader, N. Sonenberg, Translational control of hippocampal synaptic plasticity and memory by the eIF2α kinase GCN2. *Nature* **436**, 1166–1170 (2005).
59. N. T. Price, N. T. Redpath, K. V. Severinov, D. G. Campbell, J. M. Russell, C. G. Proud, Identification of the phosphorylation sites in elongation factor-2 from rabbit reticulocytes. *FEBS Lett.* **282**, 253–258 (1991).
60. N. T. Redpath, N. T. Price, K. V. Severinov, C. G. Proud, Regulation of elongation factor-2 by multisite phosphorylation. *Eur. J. Biochem.* **213**, 689–699 (1993).
61. X. Wang, W. Li, M. Williams, N. Terada, D. R. Alessi, C. G. Proud, Regulation of elongation factor 2 kinase by p90(RSK1) and p70 S6 kinase. *EMBO J.* **20**, 4370–4379 (2001).
62. E. M. Smith, C. G. Proud, cdc2-cyclin B regulates eEF2 kinase activity in a cell cycle- and amino acid-dependent manner. *EMBO J.* **27**, 1005–1016 (2008).
63. X. Wang, S. Regufe da Mota, R. Liu, C. E. Moore, J. Xie, F. Lanucara, U. Agarwala, S. Pyr Dit Ruys, D. Vertommen, M. H. Rider, C. E. Eyers, C. G. Proud, Eukaryotic elongation factor 2 kinase activity is controlled by multiple inputs from oncogenic signaling. *Mol. Cell. Biol.* **34**, 4088–4103 (2014).
64. T. A. Diggle, N. T. Redpath, K. J. Heesom, R. M. Denton, Regulation of protein-synthesis elongation-factor-2 kinase by cAMP in adipocytes. *Biochem. J.* **336**, 525–529 (1998).
65. G. J. Browne, S. G. Finn, C. G. Proud, Stimulation of the AMP-activated protein kinase leads to activation of eukaryotic elongation factor 2 kinase and to its phosphorylation at a novel site, serine 398. *J. Biol. Chem.* **279**, 12220–12231 (2004).
66. K. Griesi-Oliveira, M. S. Fogo, B. G. G. Pinto, A. Y. Alves, A. M. Suzuki, A. G. Morales, S. Ezquina, O. J. Sosa, G. J. Sutton, D. Y. Sunaga-Franze, A. P. Bueno, G. Seabra, L. Sardinha, S. S. Costa, C. Rosenberg, E. C. Zachi, A. L. Sertie, D. Martins-de-Souza, E. M. Reis, I. Voineagu, M. R. Passos-Bueno, Transcriptome of iPSC-derived neuronal cells reveals a module of co-expressed genes consistently associated with autism spectrum disorder. *Mol. Psychiatry* **26**, 1589–1605 (2021).
67. M. V. Lombardo, Ribosomal protein genes in post-mortem cortical tissue and iPSC-derived neural progenitor cells are commonly upregulated in expression in autism. *Mol. Psychiatry* **26**, 1432–1435 (2021).
68. D. S. Tylee, J. L. Hess, T. P. Quinn, R. Barve, H. Huang, Y. Zhang-James, J. Chang, B. S. Stamova, F. R. Sharp, I. Hertz-Picciotto, S. V. Faraone, S. W. Kong, S. J. Glatt, Blood transcriptomic comparison of individuals with and without autism spectrum disorder: A combined-samples mega-analysis. *Am. J. Med. Genet. B Neuropsychiatr. Genet.* **174**, 181–201 (2017).
69. T. Portmann, M. Yang, R. Mao, G. Panagiotakos, J. Ellegood, G. Dolen, P. L. Bader, B. A. Grueter, C. Goold, E. Fisher, K. Clifford, P. Rengarajan, D. Kalikhman, D. Loureiro, N. L. Saw, Z. Zhengqui, M. A. Miller, J. P. Lerch, M. Henkelman, M. Shamloo, R. C. Malenka, J. N. Crawley, R. E. Dolmetsch, Behavioral abnormalities and circuit defects in the basal ganglia of a mouse model of 16p11.2 deletion syndrome. *Cell Rep.* **7**, 1077–1092 (2014).
70. R. Luo, S. J. Sanders, Y. Tian, I. Voineagu, N. Huang, S. H. Chu, L. Klei, C. Cai, J. Ou, J. K. Lowe, M. E. Hurles, B. Devlin, M. W. State, D. H. Geschwind, Genome-wide transcriptome profiling reveals the functional impact of rare de novo and recurrent CNVs in autism spectrum disorders. *Am. J. Hum. Genet.* **91**, 38–55 (2012).

71. J. C. Darnell, S. J. Van Driesche, C. Zhang, K. Y. Hung, A. Mele, C. E. Fraser, E. F. Stone, C. Chen, J. J. Fak, S. W. Chi, D. D. Licatalosi, J. D. Richter, R. B. Darnell, FMRP stalls ribosomal translocation on mRNAs linked to synaptic function and autism. *Cell* **146**, 247–261 (2011).
72. I. Napoli, V. Mercaldo, P. P. Boyl, B. Eleuteri, F. Zalfa, S. De Rubeis, D. Di Marino, E. Mohr, M. Massimi, M. Falconi, W. Witke, M. Costa-Mattioli, N. Sonenberg, T. Achsel, C. Bagni, The fragile X syndrome protein represses activity-dependent translation through CYFIP1, a new 4E-BP. *Cell* **134**, 1042–1054 (2008).
73. R. Behringer, *Manipulating the Mouse Embryo: A Laboratory Manual* (Cold Spring Harbor Laboratory Press, ed. 4, 2014).
74. N. Murtaza, A. A. Cheng, C. O. Brown, D. P. Meka, S. Hong, J. A. Uy, J. El-Hajjar, N. Pipko, B. K. Unda, B. Schwanke, S. Xing, B. Thiruvahindrapuram, W. Engchuan, B. Trost, E. Deneault, Froylan Calderon de Anda, B. W. Doble, J. Ellis, E. Anagnostou, View ORCID Profile Gary D. Bader, S. W. Scherer, Y. Lu, K. K. Singh, Neuron-specific protein network mapping of autism risk genes identifies shared biological mechanisms and disease relevant pathologies. bioRxiv 476220 [Preprint] (2022); https://doi.org/10.1101/2022.01.17.476220.
75. J. Hui-Yuen, S. McAllister, S. Koganti, E. Hill, S. Bhaduri-McIntosh, Establishment of Epstein-Barr virus growth-transformed lymphoblastoid cell lines. *J. Vis. Exp.* , 3321 (2011).
76. K. Harb, M. Richter, N. Neelagandan, E. Magrinelli, H. Harfoush, K. Kuechler, M. Henis, I. Hermanns-Borgmeyer, F. Calderon de Anda, K. Duncan, Pum2 and TDP-43 refine area-specific cytoarchitecture post-mitotically and modulate translation of Sox5, Bcl11b, and Rorb mRNAs in developing mouse neocortex. *eLife* **11**, 11 (2022).
77. A. Shevchenko, H. Tomas, J. Havlis, J. V. Olsen, M. Mann, In-gel digestion for mass spectrometric characterization of proteins and proteomes. *Nat. Protoc.* **1**, 2856–2860 (2006).
78. Y. Perez-Riverol, J. Bai, C. Bandla, D. Garcia-Seisdedos, S. Hewapathirana, S. Kamatchinathan, D. J. Kundu, A. Prakash, A. Frericks-Zipper, M. Eisenacher, M. Walzer, S. Wang, A. Brazma, J. A. Vizcaino, The PRIDE database resources in 2022: A hub for mass spectrometry-based proteomics evidences. *Nucleic Acids Res.* **50**, D543–D552 (2022).

Acknowledgments: We thank F. Impens and R. Mayer (VIB Proteomics Core) for experimental help. We are thankful to M. Reiss and H. Kranz from Gene Bridges GmbH, Heidelberg, Germany (now Gen-H, Heidelberg, Germany) for excellent support and generating the transgenic mouse model B6;129S7-Tg(Del(7Slx1bSept1)TaoK2Hhtg/Cal. **Funding:** L.B. is supported by an FWO Postdoctoral Fellowship (12ZK221N). M.H. is partially funded by a scholarship (ID: seventh plan 2012-2017) from the Cultural Affairs and Missions Sector, Ministry of Higher Education of the Arab Republic of Egypt. N.N. was partially supported by a Deutsche Akademischer Austauschdienst (DAAD) Predoctoral Fellowship. M.K. is supported by KN556/11-1 (FOR 2419). K.E.D. was supported by Deutsche Forschungsgemeinschaft (DFG) grants DU 1396/3-1 and DU 1396/4-1 and grant 11/90 from the Werner Otto Stiftung. F.C.d.A. is supported by Deutsche Forschungsgemeinschaft (DFG) grants CA 1495/4-1 and CA 1495/7-1; ERA-NET Neuron Grants (Bundesministerium für Bildung und Forschung, BMBF, 01EW1910, and 01 EW2108B); and JPND grant (Bundesministerium für Bildung und Forschung, BMBF, 01ED1806). **Author contributions:** M.H., K.E.D., and F.C.d.A. conceived the idea, designed research, and wrote the manuscript. F.C.d.A. and K.E.D. supervised the project. M.H., T.R., R.S., M.R., Sh.H., D.P.M., B.S., and N.N. performed experiments and analyzed data. L.B., D.D., and J.d.W. performed the phosphoproteomics and proteomics from the mouse models. N.M. and K.K.S. performed the neuronal proximity–based proteomic analysis. C.K., Sö.H., and H.S. performed the proteomics from cell lines and mouse models. I.H.-B. helped to design and generated the B6;129S7-(DelSlx 1bSept1)4Aam*Tg*TaoK2Hhtg/Cal mouse line. All authors provided input for writing the manuscript. **Competing interests:** The authors declare that they have no competing interests. **Data and materials availability:** All data needed to evaluate the conclusions in the paper are present in the paper and/or the Supplementary Materials. The lymphoblast cell lines (LCLs) can be provided by S. Scherer (The Hospital for Sick Children, Toronto, Canada) pending scientific review and a completed material transfer agreement. Requests for the material transfer agreement should be submitted to: The Hospital for Sick Children ("SickKids"), 555 University Avenue, Toronto, ON M5G 1X8, Canada.

Submitted 8 November 2022
Accepted 12 March 2024
Published 12 April 2024
10.1126/sciadv.adf7001